2.1. Nanoparticles in cancer therapy

Targeting brain tumor has always been a matter of concern for researchers. Conventional delivery systems often suffered with the drawback of decreased drug concentration at site of action along with damage to non cancerous cells. Chemotherapy has been most widely used conventional system for treatment of cancer since a long time; still it suffers limitations of non selective drug distribution, unwanted toxicity and undesirable side effects to name few. These limitations led to development of new drug delivery system which could specifically target drug to tumor cells along with controlled release and targeting of drug for enhancing intracellular localization which will ultimately lead to decrease in non specific cell toxicity and side effects [1]. Nanoparticles as a drug delivery system have many advantages due to their versatile nature. The advantages include particle size and surface characteristics of nanoparticles can be easily manipulated to achieve both passive and active drug targeting. Site-specific targeting can be achieved by attaching targeting ligands to surface of the particles or by using magnetic guidance [Figure 2.1]. This will result in concomitant reduction in quantity of the drug required and dosage toxicity. It also enables the safe delivery of toxic therapeutic drugs and protection of non-targeted tissues and cells from severe side effects. This ultimately will results in an increase in the therapeutic index. Relatively high drug loading can be achieved which is very important. Controlled release can be obtained and particle degradation characteristics can be easily regulated by the choice of matrix constituents. The system can be used for various routes of administration including oral, nasal, parenteral, intra-ocular etc. Nanoparticles helps in improving bioavailability of various drugs by enhancing aqueous solubility, increasing half-life for clearance or increasing specificity for its cognate receptors [2, 3].

Among various new approaches, the use of nanoparticulate carriers for delivery of drug for cancer treatment gained attention in the last decade which led to vast research in this field. Magnetic metallic nanoparticles such as superparamagnetic iron nanoparticles (SPIOs) have been well documented for their superiority over other nanoparticles for treatment of cancer. These nanoparticles have already been approved by FDA as contrast agent for MRI of brain tumor [4]. Recent studies conducted also confirmed the efficiency of these nanoparticles for cancer treatment via hyperthermia [5].

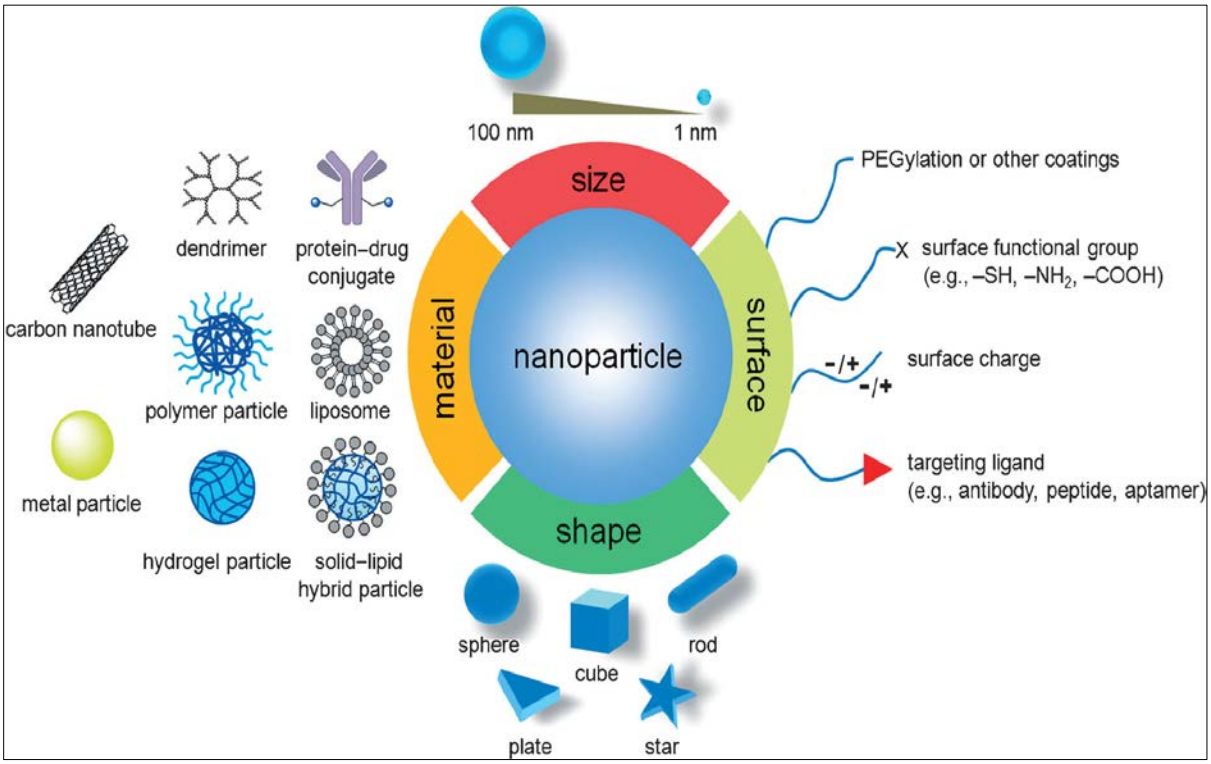

Figure 2.1: Multifunctional Metal Nanoparticles

Although iron nanoparticles have unique properties suitable for various biomedical application, unfortunately, SPIOs may undergo aggregation which might lead to changes in their magnetic properties and ultimately clinically relevant properties [6]. In the recent past, research on magnetic nanoparticles (MNP) has led to development of bimetallic or alloy nanoparticles such as FePt (Iron-Platinum), CoPt (Copper-Platinum), FeCo (Iron-Cobalt) and $SmCo_5$(Samarium-Cobalt) which possess better magnetic property and chemical stability as compared to SPIOs. Amongst bimetallic nanoparticles, FePt NPs have high Curie temperature; high saturation magnetization and high chemical stability and have magnetocrystalline anisotropy energy (206 $kJ.m^3$) much higher than SPIOs (5-10 $kJ.m^3$) [7]. Several unique chemical and magnetic properties of FePt nanoparticles makes it potential carrier for tumor targeting and treatment. Although these nanoparticles possess several advantages, still working with any type of nanoparticles has limitation with respect to thermodynamic equilibrium [7]. It is well documented that the surface to volume ratio of particles starts to increase unquestionably when we go beyond micrometer range. Same is the case with surface energy which goes on increasing and no longer remains negligible in comparison with the total energy of the system. So, to maintain state of minimum energy, continuous loss of surface energy takes place which

leads to increase in particle size [8]. Hence, nanoparticles only possess kinetic stability which is not suitable for pharmaceutical formulations

Table 2.1: List of metal nanoparticles in the market and in clinical trials

Commercial name	Compound	Function	Target disease	Development stage	Ref
Lumiren® Gastromark™	Silica-coated SPIO (Super Para-magnetic Iron Oxide nanoparticle)	MRI contrast agent	Gastrointenstinal tract and abdomen cancer	Approved marketed product	9
Sinerem	Dextran-coated USPIO (Ultra-Small Paramagnetic Iron Oxide nanoparticle)	MRI contrast agent	Lymph node tumors. Differentiation of metastatic and non-metastatic lymph nodes in patients with confirmed primary cancer.	Approved marketed product	10
Endoderm Feridex I.V.	Dextran-coated SPIO	MRI contrast agent	Liver tumors	Approved marketed product	11
Resovist®	Carboxy dextrane-coated SPIO	MRI contrast agent	Liver tumors	Approved marketed product	12
NanoTherm	Aminosilane-coated SPIO	Magnetic thermotherapy	Brain tumors. Prostate and pancreatic carcinoma.	Phase I	13
AuroShell®	Gold@silicana noshells	Photothermal therapy	Refractory head and neck Cancers. Primary and metastatic tumors in the lung.	Phase 1	14

2.2. Methods for synthesis of Metal Nanoparticles/Alloy nanoparticles

Different methods have been utilized in past for synthesis of metal nanoparticles [15]. These methods have been categorized and summarized in table 2.2.

Table 2.2: Methods for synthesis of Metal/Alloy nanoparticles

Synthetic method	**Co-precipitation method**	**Hydrothermal/ Solvothermal method**	**Thermal-decomposition method**
Precursor	For example, Ferrous salt, Ferric salt	For example , $FeCl_3.6H_2O$, $FeSO_4.(NH)_4SO_4.6H_2O$	For example, Iron acetylacetonate, Iron carbonyl, Cupferronates
Reducing agent	Not necessary	For example, Diethylene glycol	Not necessary
Stabilizer	Necessary, e.g. sodium citrate	Necessary, e.g. polyacrylic acid	Necessary, e.g. oleic acid and oleylamine
Solvent	Water	Water/ethanol	Organic compound
Reaction step	Reaction at near Room temperature followed by condensation	One step comprising liquid–solid–solid	Heating
Reaction T (˚C)	20–90	180–220	100–300
Morphology	Spheres	Disks, spheres, needles	Spheres, cubes, triangles
Size (nm)	10–50	200–800	10–30
Magnetism (emu g^{-1})	30–50	50–90	60–120
Yield	Scalable	Medium	Scalable
Advantages	Cheap chemicals; mild reaction conditions	Tunablemagnetism; tunable size; good crystallinity	Narrow size distribution; good control of the shape and crystallinity; tunable magnetism
Disadvantages	Poor control of size distribution; uncontrolled oxidation	High temperature; high pressure	Toxic organic compound; high temperature

2.3. DRUG PROFILE: LENALIDOMIDE

2.3.1. Nomenclature

a. Chemical IUPAC name: 3-(4-amino-1-oxo 1,3-dihydro-2*H*-isoindol-2-yl) piperidine-2,6-dione

b. Proprietary name: Revlimid

2.3.2. Formula

a. Empirical formula: $C_{13}H_{13}N_3O_3$

b. Molecular weight: 259.3 g/mol [16]

c. Structure

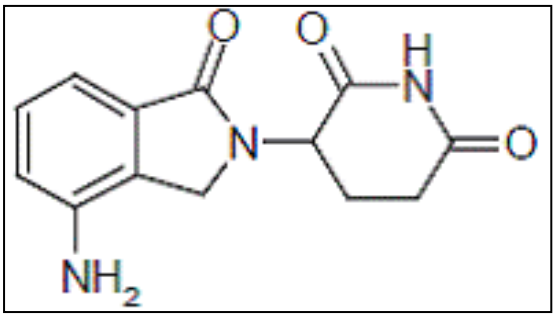

Figure 2.2: Chemical structure of Lenalidomide

2.3.3. Physicochemical properties

a. Melting point: 268.1 - 270.1 °C

b. Solubility: Water Solubility is 2.33 mg/ml. Soluble in organic solvent/water mixtures, and buffered aqueous solvents. Lenalidomide is more soluble in organic solvents and low pH solutions.

c. pKa:11.61(Strongest Acidic)/2.31(Strongest Basic)

d. log P:-0.43

e. BCS Class: III

2.3.4. Pharmacology

2.3.4.1. Drug category

Lenalidomide is the Immunomodulatory drug that is used to treat certain cancers like Multiple Myeloma (MM), Mantle Cell Lymphoma (MCL). It works by slowing or stopping the growth of cancer cells. It is also used to treat anemia in patients with certain blood/bone marrow

disorders like Myelodysplastic Syndromes (MDS).Lenalidomide may lessen the need for blood transfusions [17].

2.3.4.2. Mechanism of action

The mechanism of action of Lenalidomide remains to be fully characterized. Lenalidomide possesses immunomodulatory and antiangiogenic properties (Figure 2.2). Lenalidomide inhibits the secretion of pro-inflammatory cytokines TNF-α, IL-1β, IL-6 and IL-12 and increases the secretion of anti-inflammatoryIl-10 cytokines from peripheral blood mononuclear cells. Lenalidomide inhibits the proliferation of various hematopoietic tumor cell lines, particularly the multiple myeloma. It enhances foetal hemoglobin expression upon $CD34^+$ erythroid stem cell differentiation. Lenalidomide inhibits the expression of cyclooxygenase-2 (COX-2) but not COX-1 *in vitro*. It inhibits processes of angiogenesis including endothelial cell migration and tube formation. In addition to this, it inhibits the growth of hematopoietic tumor cells and, by inhibiting angiogenesis, reduces the growth of solid tumors *in vivo*. The molecular target of Lenalidomide is not known [18].

2.3.4.3. Indications

Lenalidomide is indicated for the treatment of patients with Multiple myeloma (MM) in combination with Dexamethasone as maintenance following autologous hematopoietic stem cell transplantation (auto-HSCT).For the treatment of transfusion-dependent anemia due to low- or intermediate-1-risk Myelodysplastic syndromes (MDS) associated with a deletion 5q abnormality with or without additional cytogenetic abnormalities. In the patients with Mantle cell lymphoma (MCL) whose disease has relapsed or progressed after two prior therapies, one of which included Bortezomib [18].

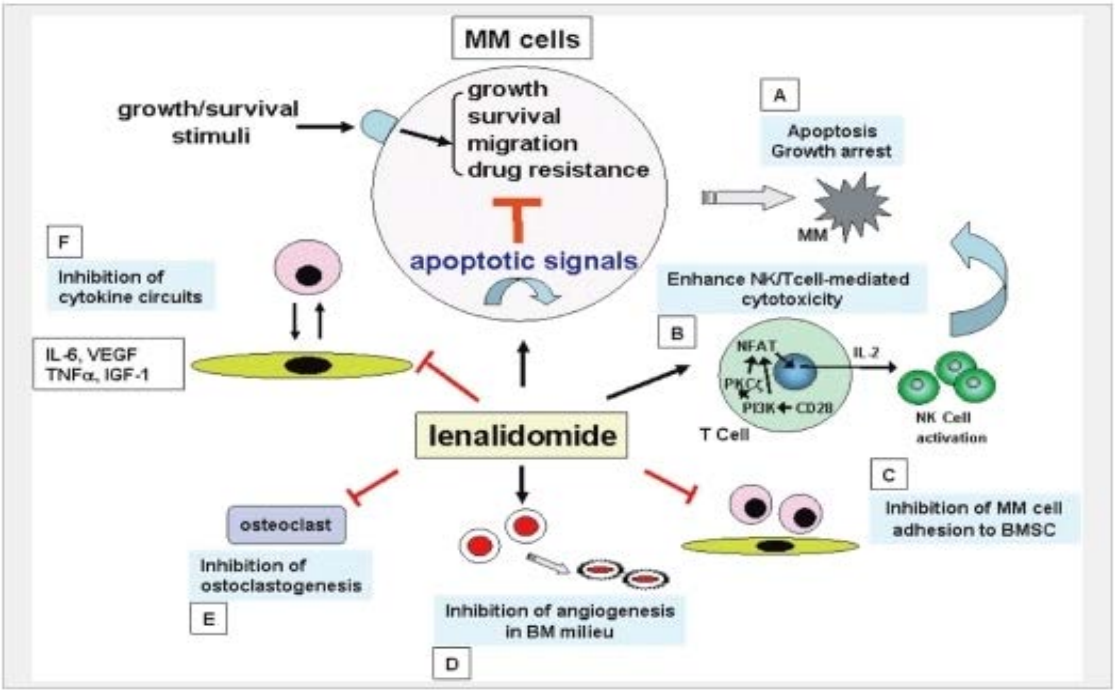

Figure 2.3: Mechanism of action of Lenalidomide

2.3.4.4. Dose and dosing frequency

a. **MM combination therapy**: 25 mg once daily orally on Days 1-21 of repeated 28-day cycle in combination with Dexamethasone.
b. **MM maintenance therapy**: 10 mg once daily continuously on Days 1-28 of repeated 28-day cycles.
c. **MDS**: 10 mg once daily.
d. **MCL**: 25 mg once daily orally on Days 1-21 of repeated 28-day cycles. In case of renal impairment the starting dose can be adjusted based on the creatinine clearance value.

2.3.4.5. Adverse reactions

Most common adverse reactions include diarrhea, fatigue, anemia, constipation, neutropenia, thrombocytopenia, leucopenia, peripheral edema, insomnia, muscle cramp/spasms, abdominal pain, back pain, nausea, asthenia, pyrexia, upper respiratory tract infection, bronchitis, nasopharyngitis, gastroenteritis, cough, rash, dyspnoea, dizziness, decreased appetite, thrombocytopenia, and tremor [19].

2.3.4.6. Contraindications

Pregnancy: Category X

In the patients who demonstrated hypersensitivity to Lenalidomide.

2.3.4.7. Drug interactions

Digoxin: Periodic monitoring of digoxin plasma levels is recommended due to increased C_{max} and AUC with concomitant Lenalidomide therapy.

Patients taking concomitant therapies such as erythropoietin stimulating agents or estrogen containing therapies may have an increased risk of thrombosis [20].

2.3.5. Pharmacokinetics

2.3.5.1. Absorption:

Lenalidomide, in healthy volunteers, is rapidly absorbed following oral administration with maximum plasma concentrations occurring between 0.625 and 1.5 hours post-dose. Co-administration with food does not alter the extent of absorption (AUC) but does reduce the maximal plasma concentration (C_{max}) by 36%. The pharmacokinetic disposition of Lenalidomide is linear. Cmax and AUC increase proportionately with increases in dose. Multiple dosing at the recommended dose-regimen does not result in drug accumulation. Oral bioavailability of Lenalidomide is <33% [20].

2.3.5.2. Distribution:

In vitro (^{14}C)-lenalidomide binding to plasma proteins is approximately 30%.

2.3.5.3. Metabolism and Excretion:

Drug undergoes limited metabolism. Two identified metabolites are hydroxy-lenalidomide and N-acetyl-lenalidomide; each constitutes less than 5% of parent levels in circulation. The cytochrome P450 enzyme system is not involved with the metabolism of lenalidomide. In healthy volunteers, approximately two-thirds of Lenalidomide is eliminated unchanged through urinary excretion. The process exceeds the glomerular filtration rate and therefore is partially or entirely active. Half-life of elimination is approximately 3 hours [20].

2.3.6. Marketed products

Only one marketed product is available.

Brand name: REVLIMID

It is available in 2.5 mg, 5 mg, 10 mg, 15 mg, 20 mg and 25 mg capsules for oral administration.

2.3.7. Drawbacks of Recent therapies

Lenalidomide suffers from atypical biodistribution; hence need to be delivered precisely at site of action. It causes side effects like Warm Auto-Immune Hemolytic Anemia (AIHA) when given via intravenous route and Bile acid Malabsorption Induced Diarrhea (BMID) when given via oral route [20].

2.3.8. Work done on Lenalidomide

Table 2.3 gives details of the research undertaken on Lenalidomide and results obtained from those experiments.

Table 2.3: Review of Research Conducted on Lenalidomide

Sr. No.	Title	Materials & Methods	Result & Conclusion	Ref.
1.	Improving the Solubility of Lenalidomide via Co-crystals	Urea and 3,5-dihydroxybenzoicacid (35DHBA). (Liquid-Assisted Grinding (LAG) method)	The solubility and bioavailability of Lenalidomide was improved via co-crystals formation.	20
2.	Lenalidomide−Gallic Acid Co-crystals with Constant High Solubility	Anhydrous gallic acid. (Liquid-Assisted Grinding (LAG) method)	After the formation of Co-crystals the solubility values increased approximately 40% in comparison with that of plain drug and the high solubility of co-crystals could remain constant within 48 h.	21
3.	Studies on drug-polymer interaction, in vitro release and cytotoxicity from chitosan particles excipient	Chitosan, Sodium hexametaphosphate (SHMP) as a cross linking agent. (Ionic gelation method)	Novel LND-CS-NPs showed sustained and effective drug release towards the target (cancer cell). Cytotoxic study revealed that LND-CS-NPs were toxic towards cancer cell lines such as MCF7 and U266.	22

2.4. Magnetic Nanoparticles

Magnetic nanoparticles (MNP) have gained lot of attention in past few decades for delivery of drugs via encapsulation or surface conjugation along with specific target molecule [23]. These nanoparticles have unique features and potential applications in biomedical science such as bio-separation and magnetic resonance imaging (MRI) [24, 25]. Amongst various MNP, superparamagnetic iron based nanoparticles (SPIOs) have been widely investigated and is the choice of magnetic material in biomedicine. Although magnetite has been approved by the Food and Drugs Administration, its use in drug delivery and biomedical field is limited due to low saturation magnetization (Ms) of around 400-500 $emu.cm^{-3}$ Hence enhancement of the magnetic moment of magnetic MNP and higher magnetocrystalline anisotropy energy than that of SPIOs in addition to narrow size distribution is the key modification required for widespread use of MNP in biomedical field [26]. To date, the most successful application of magnetic nanoparticles is for magnetic hyperthermia. A remarkable example of this involves SPIO nanoparticles, which are in a phase II study for patients with recurrent GBM in Europe. Preclinical studies indicate that magnetic hyperthermia achieved by SPIO nanoparticles can effectively promote glioma cell death and increase survival [27]. The safety and efficacy of intratumoral hyperthermia using SPIOs coated with aminosilane under a 2.5–18 kA/m and 100 kHz alternating magnetic field in conjunction with radiotherapy have been investigated in patients with recurrent GBM [28, 29]. Mixtures of magnetic nanoparticles with other imaging and therapeutic modalities have been explored in recent times (Figure 2.4).

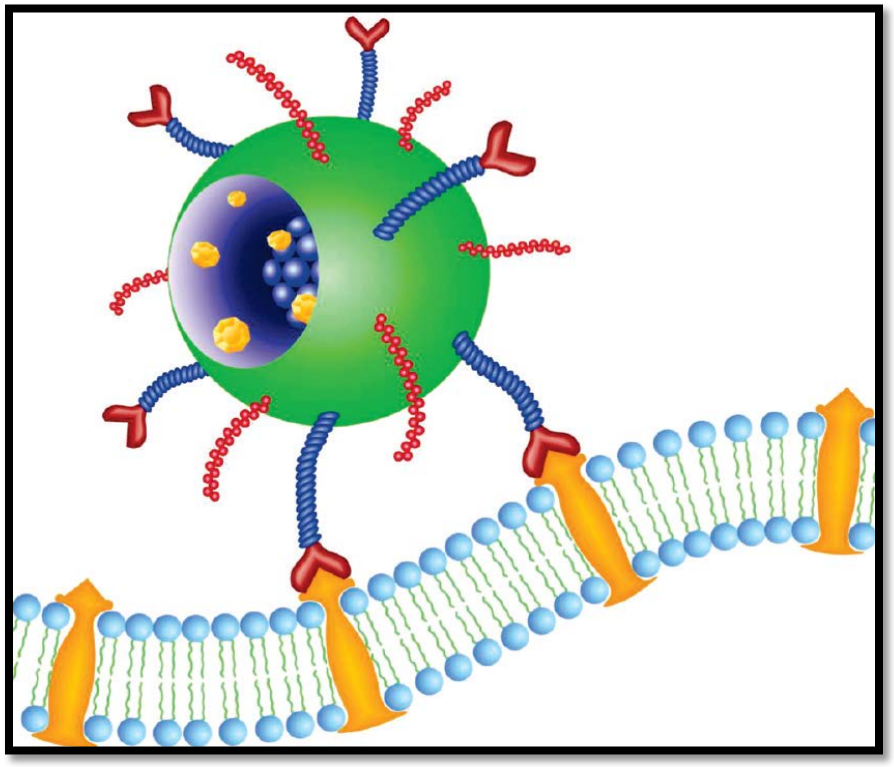

Figure 2.4**:** Multifunctional nanoparticles targeted to cancer cell membranes using a ligand to tumor cell specific surface receptor. The nanoparticles harbor an imaging (blue sphere within the core) and therapeutic agent (yellow structures within the core).

2.5. Hyperthermia

Hyperthermia refers to a procedure of raising the temperature of a part of or the whole body above normal for a defined period of time. As early as the nineteenth century, it was reported that cancer growth can be stopped by raising the temperature to higher than about 42 °C. Due to lack of blood flow and oxygen transport through the newly formed immature blood vessels within tumors, tumors residing in an acidotic and nutrient-deprived environment have a greater thermosensitivity. The temperature elevation associated with hyperthermia is about a few degrees above normal body temperature at 41–45 °C [30]. The main mechanism for tumor damage at temperature above 41 °C is probably protein denaturation, which causes alterations in cytoskeleton and membrane structures and changes of enzyme complexes for DNA synthesis and repair. Hyperthermia is a potent sensitizer of cell killing by ionizing radiation, which can be attributed to the fact that heat can inhibit radiation-induced DNA damage repair and improve

oxygenation to limit the degree of hypoxia that hampers the effectiveness of radiotherapy. As a radio sensitizer, hyperthermia can enhance the biology effect of radiation and reduce the dosage of radiation for cancer treatment [31]. Experimental results for magnetic fluid hyperthermia (MFH) with iron oxide particles have been promising. The pilot clinical studies regarding magnetic fluid hyperthermia in prostate carcinoma were reported ealier [32]. A patient with prostate cancer received direct tumor injection of aminosilane-coated iron oxide nanoparticles. Thermal treatments of 60 minutes once a week were delivered to the patient for 6 weeks. CT scans indicated that the nanoparticles were retained in the prostate for the entire 6-week period. No systemic toxicity was detected at a median follow-up after one year. FePt nanoparticles have several advantages over iron nanoparticles as discussed above and hence will be therapeutically more effective in comparison to iron nanoparticles. Apart from hyperthermia generation, various nanoparticle constructs containing magnetic elements such as iron, gadolinium, and manganese are in development or have already made their way to a clinical setting for use as MRI contrast agents in the imaging of brain tumors [33]. These nanoparticles have been shown to increase signal enhancement for a long period of time and enhance visualization of the tumor border. Iron oxide nanoparticles have been extensively studied as T2/T2* contrast agents for brain tumor imaging. Ferumoxytol, an ultra-small SPIO coated with polyglucose sorbitol carboxymethyl ether, has been used as the MRI contrast agent together with a standard gadolinium chelate for patients with recurrent high grade glioma receiving chemotherapy in phase I clinical trials (ClinicalTrials.gov Identifier: NCT00769093) [34]. Quantitative imaging changes of brain tumor vascularity after anti-angiogenic therapy with bevacizumab versus steroid therapy with dexamethasone are being assessed by a dual agent MRI study using gadolinium and ferumoxytol. PEGylated SPIO nanoparticles possessing a surface-bound brain tumor targeting peptide chlorotoxin (CTX) that showed high selectivity and binding affinity to membrane-bound matrixmetalloproteinase-2 (MMP-2) in gliomas [35]. Copper^{67} conjugated metal nanoparticles have been explored for PET imaging in combination with MRI. FePt nanoparticles can also be explored as potential MRI contrast agent. Previous reports have confirmed use of FePt as contrast agent. Further modification in FePt nanoparticles along with little surface modification can be useful for multimodal imaging of tumors using FePt nanoparticles. While the magnetically active FePt nanoparticles are responsible for magnetic retention, the nanoparticle surface properties determine the particle interaction with both the payload and the physiological

milieu. Surface charge appears to be especially important with regards to these interactions. In particular, cationic nanoparticle surface was shown to present several drug/gene delivery advantages over its anionic and electroneutral counterparts. For example, magnetic nanoparticles functionalized with a polycationic polyethyleneimine (PEI) were demonstrated to bind DNA and act as efficient transfection agents in vitro. In addition, a positive surface charge was reported to enhance nanoparticle cellular uptake and confer strong avidity towards the anionic proteoglycans in tumor vasculature. Various polymers have been employed for conjugation on nanoparticles with the aim of enhancing target specificity. Hyaluronic acid is one of the few biodegradable polymers often used to impart CD44 specificity to nanoparticles but it suffers the disadvantage of inducing tumor invasion driven by important molecular events including matrix metalloproteinase (MMP) secretion and upregulation of cell migration. MMP secretion is triggered by HA-induced focal adhesion kinase (FAK) activation, which transmits its signal through ERK activation, nuclear factor kappa B (NFκB) translocation and fibrin polymerization [36, 37]. Hence, it is important to keep this point in mind while utilizing HA as CD44 specific targeting ligand.

2.6. Photothermal Therapy

Various metal based nanomaterials such as titanium dioxide (TiO_2) possess a photosensitive property which has been explored as therapeutic agents for light-mediated treatment of brain tumor [38, 39]. Upon light exposure, these nanoparticles absorb energy from the incident light and transfer it to molecular oxygen which leads to generation of a variety of cytotoxic reactive oxygen species (ROS) which further reacts with essential cellular components such as DNA, proteins, and lipids [40, 41]. Gold nanoparticles including gold nanoshells and nanorods have demonstrated conversion of absorbed NIR light to heat followed by induction of cell death [41, 42]. Gold coated silica nanoshells in which a 120 nm diameter silica core was coated by a 10–20 nm thin layer of gold, was investigated for their photothermal ability. The obtained results demonstrated successful targeted ablation of glioma cells in vitro and in vivo that under NIR laser light excitation in a subcutaneous implanted U373 glioma mouse model [43]. PDT using conventional photosensitizers has been tested on the clinical setting for brain tumors as an intraoperative adjuvant therapy (ClinicalTrials.gov Identifier: NCT01682746, NCT00118222, NCT01148966).

2.7. FePt Alloy Nanoparticles

Recent research on MNP has led to development of bimetallic or alloy nanoparticles such as FePt, CoPt, FeCo and SmCo5 which possess better magnetic property and chemical stability as compared to SPIOs. FePt nanoparticles have Ms of about 1000 emu.cm^{-3}. With higher MS, MNP experience higher driving forces under a magnetic field, and thus, the efficacy of drug delivery or magnetic separation will be greatly improved. FePt NPs have high Curie temperature, high saturation magnetization and high chemical stability. Due to high value of Ms, FePt nanoparticles also hold great potential for being used as multifunctional MNP for simultaneous drug delivery and hyperthermia therapy. In case of FePt, the magnetocrystalline anisotropy energy is 206 kJ.m3, which is much higher than SPIOs (5-10 kJ.m3) [44]. The hyperthermia generated by FePt can further be modulated by optimizing the size of nanoparticles as an increase in magnetocrystalline anisotropy energy is observed with decrease in particle size of MNP [44, 45]. Owing to its unique magnetic and chemical properties, FePt nanoparticles are being investigated for tumor targeting and treatment. The use of FePt nanoparticles for tumor targeting further depends on chemical composition and colloidal stability of these nanoparticles. Xu et al. reported that FePt nanoparticles undergo leaching in acidic environment to release Fe which acts as cytotoxic agent by catalyzing decomposition of hydrogen peroxide (H2O2) into reactive oxygen species (ROS) inside cell which ultimately leads to cellular damage [46]. Hence variation in composition of FePt nanoparticles will elucidate variation in cellular cytotoxicity. These metallic nanoparticles have been investigated for delivering drug to tumor cells for utilizing the combined advantage of targeted drug delivery, hyperthermia and MRI of tumors [47-49]. Surface functionalization of these nanoparticles have been done in past to enhance biocompatibility along with introduction of various functional groups for surface conjugation using different ligands and drugs [50, 51]. Such functionalization helps in development of nano-carriers for multimodal therapy and imaging of tumors. The multimodal therapy of tumors includes treatment of tumors via multiple pathways which may or may not be limited to presence of anticancer agents alone or in combination, but include nano-carrier mediated tumor therapy such as hyperthermia, production of ROS, DNA damage etc [52-55]. Such multimodal therapy has proven to be more effective in comparison to mono-therapy or bimodal therapy. A research involving comparison of bimodal therapy and trimodal therapy concluded trimodal therapy to be

more effective against locally advanced small cell lung cancer [56]. FePt alloy nanoparticles have recently gained a lot of importance and have been selected for clinical phase II trials for hyperthermia and imaging of tumor [57]. Stoichiometric FePt alloy has two phases one of which is face-centered cubic (fcc) and the other one is face-centered tetragonal (fct) or L10 structure [58]. In the disordered fcc structure, the probability of face and corner sites being occupied by a specific type of atom is the same. L10 is a crystallographic derivative structure of the fcc structure and has two of the faces occupied by one type of atom and the corner and the other face occupied with the other type of atom [59]. Therefore, L10 phase is usually called the ordered phase. The disordered to ordered (fcc to L10) transformation will introduce translational domains (also called anti-phase domains), orientational domains (also called variants or merohedral twins) and magnetic domains. The first two types of domains are produced by the lowering of translational and point symmetry. The magnetic domains are due to the transformation from paramagnetic to ferromagnetic domains. The L10 phase of FePt is stable at the temperature less than 1300℃. The fcc to L10 transformation is a first-order transformation but the reaction can happen homogeneously and continuously when the reaction temperature is away from the equilibrium phase boundary and below the instability temperature.

2.7.1. Magnetic Properties of FePt

The face-centered cubic (fcc)-structured FePt has a small coercivity and is magnetically soft. The fully-ordered FePt with L10 structure has Fe and Pt atom layered alternating along the x direction. The anisotropy constant K measures the ease of magnetization reversal along the easy axis. Compared to known rare earth elements based alloys, FePt with L10 structure has a very high anisotropy energy (up to 6.6×107 erg/cc) and high resistance to oxidation [60, 61]. The large anisotropy is due to Fe and Pt interactions from the spin-orbit coupling and the hybridization between Fe 3d and Pt 5d states. Meanwhile, the Fe-Pt interatomic interaction makes the FePt nanoparticles more chemically stable compared with the common high-moment nanoparticles of Co and Fe, as well as the large coercive materials of SmCo5 and $Nd_2Fe_{14}B$. Its anisotropy constant K, which measures the ease of magnetization reversal along the easy axis, can reach as high as 107 Jm^{-3}, a value that is one of the largest among all known hard magnetic materials [62]. This large K is caused by Fe and Pt interactions originating from spin-orbit coupling and the hybridization between Fe 3d and Pt 5d states [63-66]. These Fe–Pt interactions

further render the FePt nanoparticles chemically much more stable than the common high moment nanoparticles of Co and Fe, as well as the large coercive materials $SmCo_5$ and $Nd_2Fe_{14}B$, making them especially useful for practical applications in solid-state devices and biomedicine.

2.7.2. Surface Functionalization of FePt Nanoparticles

Synthesized magnetic nanoparticles employed in biomedical field should possess few properties such as high chemical stability, excellent dispersion, and biocompatibility. These properties are generally not found in metal nanoparticle which makes it hard for researchers to explore their biomedical applications. The most commonly explored method for enhancing stability of magnetic nanoparticles (MNPs)/metal nanoparticles is surface modification [67]. Surface modifications include addition of ligand, exchange of ligand, chemical conjugation, and bioconjugation. The efficiency of surface modification affects various physical and chemical stability properties of magnetic nanoparticles as it not only effectively reduce the surface energy needed to obtain MNPs with excellent dispersion but also can improve the biocompatibility of the MNPs. Introduction of reactive functional groups on the surface of MNPs further provides options for conjugation of other ligands making it multifunctional nanoparticles. Various ligand have been used for surface modification of MNPs such as 2-amino ethyl mercaptan, aspartic acid, glutamic acid, citric acid, phosphorus acid, vitamin B, and gamma cyclodextrin, glucose, starch, polyethylene glycol (PEG), polyethyleneimine (PEI), polypeptides, proteins, and polyvinyl alcohol (PVA) [68-72]. Chou et al. conjugated cysteamine-FePt MNPs with an anti-Her2 antibody and confirmed that the modified nanoparticles for the imaging contrast had excellent biocompatibility and hemocompatibility [73]. Working on similar line, Chen et al. obtained cysteamine surface functionalized FePt nanoparticles with good biocompatibility and high chemical stability [74]. Similarly, Silica and (3-aminopropyl) triethoxysilane were used to functionalize the surface of FePt nanoparticles which exhibited good biocompatibility and stability.In another experiment, Chen et al. used mercaptopropionic acid to produce COOH terminated, water-dispersible FePt nanoparticles. The COOH-FePt nanoparticles were then activated using N-ethyl-N 8- (dimethylaminopropyl)-carbodiimide (EDC) followed by conjugation of folic acid to provide target specificity to nanoparticles. The final FePt nanoparticles had excellent biocompatibility and photothermal transduction efficiency [75]. Liu

et al. used PEG to functionalize FePt@Fe_2O_3 core-shell nanoparticles and conjugated folic acid to the surface of the functionalized FePt@Fe_2O_3-PEG nanoparticles. The synthesized nanoparticles demonstrated high stability in diverse physiological solutions [76]. In another modification, Fuchigami et al. utilized poly (diallyldimethylammonium chloride)- (PDDA-) to modify silica particles as a template to produce PDDA-modified silica particles coated with FePt nanoparticles. The silica layer was then dissolved in a NaOH solution to obtain FePt-nanoparticles/polycation hybrid capsules, having superior capacity to carry drugs and genes [77].

2.7.3. Biocompatibility and Safety

Biocompatibility of nanoparticles is one of the prerequisite for their use in biomedical purpose. The assessment of FePt nanoparticles cytotoxicity is a key factor which needs to be considered before estimating their potential in biomedical field. The most commonly used method for analysis of cytotoxicity is use of diverse cell lines [78].

FePt nanoparticles were incubated with A375M, MCF7, and U2OS cell lines for 168 h to analyze their cellular toxicity. The result demonstrated absence of cytotoxicity even after 168 hours of incubation and no cytotoxicity was observed at nanoparticle concentrations below 30 μg/mL [79]. In another similar study, Chou et al. used MTT assay, hemolysis test, and biodistribution analysis for evaluating the biocompatibility of FePt nanoparticles. The results showed absence of any significant cytotoxicity (cell viability >90%) at Fe concentrations below 10mM, and the cell viability was as high as 75% at the highest concentration of nanoparticles (100 mM). No significant hemolysis (<5%) was observed at 100mM Fe concentrations of FePt nanoparticles. The results of biodistribution study in 6-week-old male C3H/HeN mice demonstrated that most of the particles were mainly accumulated within the spleen followed by lung and liver [80]. In another work, cytotoxicity of FePt@Fe_2O_3-PEG core-shell nanoparticles was assessed using MTT assay in KB cells along with the lactate dehydrogenase (LDH) leakage assay to determine the cell membrane integrity [81]. The results obtained demonstrated no clear cell membrane damage induced by the synthesized nanoparticles even after 3 days of incubation. The *in vivo* animal study showed absence of potential toxicity in nanoparticle-treated mice, death and notable abnormalities were absent at the tested dose of 34mg/kg of Fe for 20 days and no obvious damage, lesion, or inflammation in major organs was observed in stained tissue slices.Liang et al. used an MTT assay to evaluate the cytotoxicity of their synthesized FePt-Cys

nanoparticles in the ECV304, L929, and HEK293 cell lines. Compared to the control group, no striking differences in cell viability were observed in the FePt-Cys nanoparticle-treated group [82].

2.7.4. Biomedical Application of FePt Nanoparticles

FePt nanomaterials have been employed in various biomedical fields such as biosensing, targeted drug delivery, MRI, fluorescence imaging, and therapy experiments. Some biomedical applications of functionalized FePt MNPs are shown in Figure 2.5.

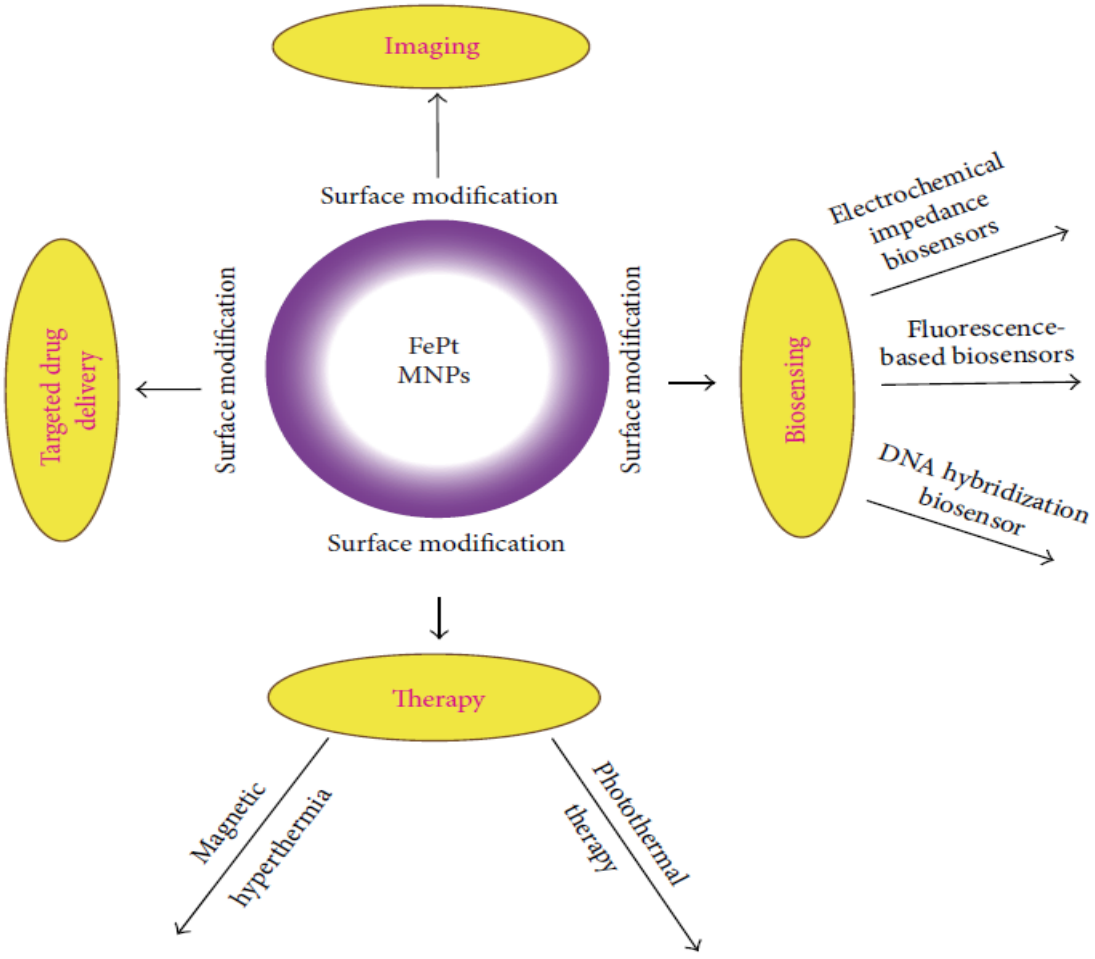

Figure 2.5: Biomedical application of FePt nanoparticles

Table 2.4: Applications of magnetic nanoparticles in cancer treatment

NP core composition	NP coating	Size	Drug	Targeting ligand	Cell/in vivo model	Application	Ref.
Bismuth-iron oxide composite	Dextran	98 nm	None	None	Human liver carcinoma cells (Hep G2) BJ5ta fibroblasts C57BL/6J mice	Dual CT and MRI T_2 contrast agents were successfully deployed in an in vivo murine model	83
Iron oxide	PEG	10 nm	None	None	J774 macrophages	SPIONs capable of enhancing T_1 contrast in MRI were developed and tested in vivo	84
18F-iron oxide composite	Dextran	30 nm	None	None	BALB/c mice	Trimodal imaging contrast agents providing MRI, PET, and CT capabilities were evaluated in vivo	85
Iron oxide	Chitosan	50 nm	Temozolomide	Chlorotoxin	Glioblastoma cells (U-118 MG) C57BL/6J mice	Drug delivery vehicles capable of carrying the chemotherapeutic temozolomide specifically to glioblastoma brain cancer cells were tested in vitro	86
Iron oxide	PEI	100 nm	siRNA targeting human telomerase reverse transcriptase	None	MCF-7 cells PC3 cells SKOV-3 cells Hep G2 cells BALB/c mice with Hep G2 xenograft tumors	Redox-sensitive gene and siRNA delivery was achieved in vitro and in vivo to induce apoptosis and inhibit growth of liver cancer	87
Iron oxide	Chitosan PEG PEI	40 nm	Apurinic endonuclease 1 suppressing siRNA	None	Medulloblastoma cells (UW228-1) Ependymoma cells (Res196)	In vitro delivery of siRNA to two types of brain tumor cells was facilitated by iron oxide NPs; the siRNA reduced the activity of an enzyme implicated in radiation resistance in tumors	88

Iron oxide	PEG	19 nm	None	None	Immunodeficienta thymic NMRI mice Human epidermoid carcinoma xenografts (A431 cells)	SPIONs injected intratumorally into skin cancer xenografts induced localized hyperthermia when irradiated with an external magnetic field, arresting tumor growth	89
Iron oxide	PVA	75–200 nm	Doxorubicin Paclitaxel	IVO24 peptide	Human cervical carcinoma cells (HeLa) Human breast carcinoma cells (MCF-7) Mice bearing MCF-7 tumors	Dual-drug loaded, therapeutic delivery vehicles that release drugs upon exposure to an external magnetic field were used to treat breast and cervical cancer models in vitro and in vivo	90
Gold-iron oxide composite	PEG	25 nm	None	A33 scFv antibody	Colorectal cancer cells (SW1222 and HT 29)	Active targeting of colorectal cancer cells and subsequent selective photothermal ablation of tumor tissue in vivo	91
Iron oxide	APTES	15 nm	Pheophorbide-A	None	Epithelial cancer cells (KB cells)	Simultaneous photodynamic therapy and dual-mode fluorescence/MR imaging of epithelial cancer cells in vitro was demonstrated	92
Iron oxide	PEG	100 nm	Chlorin e6	None	Murine breast cancer cells (4T1) BALB/c mice	In vitro and in vivo photodynamic therapy was used to treat breast cancer in a murine model; cancer tissue was specifically targeted by drawing NPs to tumor sites via an external magnetic field	93

2.7.4.1. As Contrast Agent for MRI and Probe for Fluorescence Imaging

FePt-A and FePt-silica-A nanoparticles were investigated for their use as MRI contrast agents. The obtained r^2 values were 887mM^{-1}·s^{-1} and 210mM^{-1}·s^{-1} for fcc-FePt-A and fcc-FePt-silica-A nanoparticles, respectively, in the MRI magnetic field (7 T), whereas the $r2$ value of commercial Feridex was 148mM^{-1}·s^{-1}.Their work demonstrated that the FePt-based T2 contrast agents were superior to commercial Feridex with respect to MRI contrast enhancement [94]. In another similar experiment, Gao et al. described FePt@Fe_2O_3 core-shell nanoparticles for MR imaging. Compared to commercially available iron nanoparticles (MION ($r2$ = 2.778 (μg/mL) $^{-1}$ s^{-1}) and Sinerem ($r2$ = 2.450 (μg/mL) $^{-1}$ s^{-1})), as-synthesized FePt@Fe_2O_3 yolk-shell nanoparticles ($r2$ = 3.462 (μg/mL) $^{-1}$ s^{-1}) exhibited stronger contrast enhancement and could act as a potential MRI contrast agent [95]. Size-tunable superparamagnetic FePt nanoparticles were investigated for their potential as a dual-modality contrast agent for CT/MRI. The obtained results showed that superparamagnetic FePt nanoparticles could enhance shortening of the T2 of proton relaxation and produce efficient CT contrast enhancement [96]. In an experiment, using a one-pot synthesis procedure, superparamagnetic FePt@CdX core-shell nanocrystals (X = S or Se) was synthesized which could show fluorescence with quantum yield of 2.3–9.7% [97]. Similarly, FePt core-shell nanoparticles was synthesized using fluorescent dye NOPS. The nanoparticles displayed fluorescence in ethanol (EtOH) [87]. Taylor et al. reported encapsulation of superparamagnetic FePt nanoparticles with PEGylated phospholipids to form stealth immunomicelles for specifically targeting of human prostate cancer cells which can be detected by MRI and fluorescence imaging [98].

2.7.4.2. Magnetic Fluid Hyperthermia (MH) and Photothermal Therapy

Under an external alternating magnetic field (AMF), the magnetic fluid in tumor tissue or cells is heated through the main mechanisms of Brownian and N´eel relaxation, and then the produced heat kills the tumor. This process is called MH. The use of FePt nanoparticles as a medium for MH has been explored in the last two decades. Theoretical assessment of MH produced by FePt MNPs was done and was found that these FePt MNPs displayed great superiority to magnetite, maghemite, FeCo, and L10 FePt MNPs in MH [99]. At $H0$ = 50mT and f = 300 kHz, the energy dissipation of 9 nm fcc FePt MNPs was $P = 3.97 \times 10^5$ W/m, while the

energy dissipation of 19nm magnetite MNPs was only P = 1.95 ×105 W/m. In a similar experiment, tungsten-oxide coated biocompatible FePt core-shell nanoparticle demonstrated approximately 3^0C increase in the aqueous suspension after 15min in 831 kHz high-frequency AMF of 250 Gauss field strength (25mT) at a moderate nanoparticle concentration (0.5mg/mL) [100]. In case of photothermal therapy, the photothermal effect of folate functionalized FePt nanoparticles activated by a NIR femtosecond laser was examined [101]. Due to their superior photothermal transduction efficiency, these nanoparticles heated up to several hundred degrees Celsius in picoseconds under laser irradiation.

2.7.4.3. FePt Nanoparticles as Drug Delivery Carrier

Porous FePt capsules were explored as a magnetically targeted drug delivery system. Anticancer drug was loaded in the porous nanoparticles and was coated with lipid membrane to avoid leaking of the agents, the magnetic capsules arrived at lung cancer cells and gastric cancer cells within 15 min under a NdFeB magnet (0.2 T), resulting in greater than 70% cancer cell death [102]. For controlling drug release, DOX loaded FePt@Fe_2O_3-PEGFA nanoparticles were prepared and incubated in buffers with pH values of 7.4 and 5.0 to assess their drug release behaviors [103]. After 24 h of incubation, it was observed that approximately 1.5% DOX was released at pH 7.4 and approximately 20% DOX was released at pH 5.0, indicating accelerated release at a lower pH value. Apart from being used as drug delivery carrier, FePt nanoparticles themselves behave as anticancer agent. Studies have shown that FePt MNPs can suppress the proliferation of some cancer cells. It was reported that according to an MTT assay, FePt@CoS_2 yolk-shell nanocrystals showed an IC50 of 35.5 ± 4.7 ng of Pt/mL in HeLa cells, which was considerably lower than that of cisplatin (230 ng of Pt/mL) [104]. In another research it was reported that FePt nanoparticles functionalized with the *luteinizing hormone-releasing hormone* (*LHRH*) peptide could take precedence in binding to A2780 and suppress the proliferation of these tumor cells. Their work demonstrated that these functionalized FePt nanoparticles could be a new agent for controlled cancer therapy [105].

2.8. Polyethylenimine

It has been shown that cationic polymers such as poly-arginine enhance nasal absorption of a hydrophilic model drug by acting on the tight junctional protein ZO-1. PEI also belongs to family of cationic polymers carrying positive surface charges that interact with the negatively

charged cell membrane, are readily endocytosed by many cell types. It has been reported that similar to poly (arginine), PEI increases drug absorption by increasing paracellular permeability [106, 107]. *In vitro* study using liposomes made of phospahtidyl serine demonstrated that bPEI caused more destruction of liposomal membrane as compared to lPEI [108]. This suggests that PEI can destabilize or disrupt plasma membrane. In a study conducted to analyze stress and toxicity pathways triggered by PEI, it was observed that endocytic uptake of PEI caused swelling and rupture of endosomes causing intracellular stress and mitochondrial alterations, finally leading to apoptotic cell death at higher doses [109]. Previous research has shown that PEI is able to depolarize mitochondria leading to increased caspase-9 activity, decreased mitochondrial membrane potential, and increased phosphatidylserine exposure as early as one hour after treatments with PEI polyplexes at an N/P ratio of 5 [110-112]. Abovementioned facts give us insight about possible synergistic effect which might be obtained with respect to disruption of mitochondrial functions. PEI also provides nanoparticles the ability to deliver gene and protein/peptides for combination drug therapy. The conjugation of PEI with metals has opened a new avenue in field of PEI based systems. Such systems have demonstrated to provide diagnostic as well as imaging capability of PEI based systems in addition to therapeutic ability. The result obtained for magnetic PEI vectors have shown to be effective in monitoring and imaging the targeting of PEI based vectors. Such system can enhance the targeting efficiency as well as help to study the cellular internalization [113]. Li and coworkers fabricated PEI based theranostic nanoparticles using iron oxide nanoparticles [114]. Magnetic iron oxide-based nanoparticle comprising a magnetic inner core and a disulfide-containing polyethylenimine (SSPEI) outer layer was synthesized, for redox-triggered gene release in response to an intracellular reducing environment. The results of this study demonstrated the potential of a disulfide-containing PEI-decorated magnetic nanoparticle as highly potent and low-toxic theranostic nano-system for specific nucleic acid delivery inside cancer cells. Similar work had been reported using 3-(2-aminoethylamino) propyltrimethoxysilane modified magnetic nanoparticles [115]. These modified magnetic nanoparticles were further conjugated to PEI-folic acid (PF) conjugate. The formed theranostic nanoparticles demonstrated feasibility as contrast agents in magnetic resonance imaging (MRI) and as gene carriers for gene delivery. Apart from being contrast agent, these nanoparticles demonstrated specific cellular uptake by KB cells usingWI-38 cells as comparison by confocal microscopy. Mesoporous silica nanoparticles were

functionalized with cyclodextrin grafted PEI. Pyruvate kinase M2 isoform (PKM2), (which is overexpressed in several cancer types), was used as a target gene to evaluate the effectiveness of developed mesoporous silica nanoparticles based delivery system [116]. Cellular internalization, subcellular localization, gene silencing capability and anticancer activity of siRNA-loaded nanoparticles were assessed with MDA-MB-231 human breast cancer cells.

Recently, PEI based nucleic acids have been investigated for ocular delivery. Delivery of nucleic acids through intravenous administration is associated with poor pharmacokinetics arising out of blood-aqueous barrier in the anterior part of the eye and blood-retinal barrier in the posterior part of the eye [117, 118]. Subretinal injection is being employed in the current ongoing gene therapy trials for RPE65-associatedLeber's congenital amaurosis [119]. Pullulan modified PEI was used for targeting siRNA to liver. Results suggest that the PEI-pullulan polymer may be a useful, low toxic means for efficient delivery of siRNA into the liver [120]. PEI modified with poly (L-lysine) using PLL copolymers were synthesized with different molecular weights and ratios of PEI. Luciferase assay was used to demonstrate the gene transfection efficiency of pDNA-polymer to Neuro2A cell line. DNA condensation and particle size measurements showed that new PLL-PEI conjugates could form polyplexes in nano-scale size in the range of 99–122 nm and were able to condense DNA at low concentration. While cytotoxicity reduced in some groups, the transfection efficiency increased about 2.8and 4 fold as compared to the unmodified PEI 1.8 kDa and 10 kDa, respectively [121]. In another modification, tyrosine-modified low-molecular weight polyethylenimine was synthesized for efficient siRNA delivery. The comparative results with the respective parent PEI reveals that knockdown efficacies were significantly enhanced by the tyrosine modification, as determined in different reporter cell lines, without appreciable cytotoxicity [122]. Exploring the application of PEI in wound dressings, a study was conducted to establish structure-property relationship between linear and branched polyethylene imines by examining their antimicrobial activities against wide range of pathogens [123].The results obtained from simulation results suggested that LPEI forms weak complex with the zwitterionic lipids whereas the side chain amino groups of BPEI sequester the zwitterionic lipids by forming tight complex. Crosslinking of BPEI onto electrospun gelatin mats attenuated the cytotoxicity for fibroblasts while retaining the antimicrobial activity against Gram-positive and yeasts strains. PEI crosslinked gelatin mats elicited bactericidal activity by contact-mediated killing and were durable to leaching for around

7 days. A novel pulmonary delivery system of siRNA, transferrin-polyethylenimine (Tf-PEI), was designed to selectivelydeliver siRNA to ATCs in the lung. Biodistribution of polyplexesin a murine asthmatic model confirmed that Tf-PEI polyplexes can efficientlyand selectively deliver siRNA to ATCs [124]. Ramezani and coworkers covalently attached to poly(ethylene glycol) (PEG) and polyethylenimine (PEI) 10 kDa, or its derivatives to carbon nanotubesfor using it as a carrier for gene delivery along with conjugation of5TR1 aptamer to enhance tumor specificity [125]. PEI 10 kDa or its alkyl carboxylate derivatives were conjugated to SWCNT-PEG to develop vectors possessing effective DNA condensation ability which can interact with cell membrane via both nano-needle mechanism and electrostatic interactions produced by SWCNT and PEI, respectively. The results demonstrated that SWCNT-PEG-PEI and SWCNT-PEG-derivatives of PEI could condense DNA into particle size less than 150 nm with positive surface charges. Apart from nucleic acid delivery, modified PEIs have also been investigated for diagnostic and imaging purposes. Epsilon caprolactone modified PEI was explored for simultaneous antigen delivery and for MRI purpose. It was found that PEI-Caprolactone demonstrated as a chemical exchanges aturation transfer contrast agent for magnetic resonance imaging [126].Similarly, PEI along with barium titanate was recently reported for gene delivery and coupled imaging [127]. Bio-reducible polyethylenimine/siRNA complexes conjugated with N-acetylglucosamine as a targeting moiety has been used for therapy of activated hepatic stellate cells (HSCs) and fibrotic liver tissue and simultaneous imaging of liver fibrosis. Results indicated that the above synthesized PEI complex can be potentially used for simultaneous therapeutic and imaging [128]. In another study, fluorescent organic nanoparticles were synthesized with a quantum yield of about 14% using polyethylenimine and sucrose [129]. The synthesized nanoparticles demonstrated intense fluorescence, excitation-dependent emission feature, excellent nanoparticle stability, and high photostability. These results demonstrate that PEI can be used as potential surface modifying agent owing to its unique properties supporting drug delivery as well as targeting.

2.8.1. Review of Literature on PEI Based Nanocarriers:

Ding Y., et al., 2015 proposed novel approach for fabrication of hydrogel based on chitosan (CS) crosslinked carboxymethyl-β-cyclodextrin (CM-β-CD) polymer modified Fe_3O_4 magnetic nanoparticles was synthesized for delivering hydrophobic anticancer drug 5-fluorouracil (CS-

CDpoly-MNPs). Carboxymethyl-β-cyclodextrin being grafted on the Fe_3O_4 nanoparticles (CDpoly-MNPs) contributed to an enhancement of adsorption capacities because of the inclusion abilities of its hydrophobic cavity with insoluble anticancer drugs through host–guest interactions. The nanocarriers exhibited a high loading efficiency (44.7 ± 1.8%) with a high saturation magnetization of 43.8 emu/g. UV–Vis spectroscopy results showed that anticancer drug 5-fluorouracil (5-Fu) could be successfully included into the cavities of the covalently linked CDpoly-MNPs. Moreover, the free carboxymethyl groups could enhance the bonding interactions between the covalently linked CDpoly-MNPs and anticancer drugs. *In vitro* release studies revealed that the release behaviors of CS-CDpoly-MNPs carriers were pH dependent and demonstrated a swelling and diffusion controlled release. A lower pH value led to swelling effect and electrostatic repulsion contributing to the protonation amine impact of NH3+, and thus resulted in a higher release rate of 5-FU. The mechanism of 5-FU encapsulated into the magnetic chitosan nanoparticles was tentatively proposed. A novel nanocarrier, chitosan-coated magnetic drug carrier nanoparticle (CS-CDpoly-MNPs) is fabricated for the delivery of insoluble anticancer drug by grafting CM-β-CD onto the magnetite surface. The grafting of CM-dextrins onto the surface of Fe_3O_4 nanocrystal clusters can markedly increase the loading capacity of 5-FU by virtue of CM-dextrins/5-FU inclusion complex formation. The release of 5-FU from nanocomposite carriers was pH dependent and displays different release efficiencies in various release media solutions [130].

Huang J., et al., 2015 explored the potential of drug delivery system composed of layer-by-layer (LBL) milk protein casein (CN) coated iron oxide nanoparticles. Doxorubicin (DOX) and indocyanine green (ICG) were selected as model drug molecules, which were incorporated into the inner polymeric layer, and subsequently coated with casein. The resulting casein coated iron oxide nanoparticles (CN-DOX/ICG-IO) were stable in the acidic gastric condition with the presence of gastric protease. On the other hand, the loaded drugs were released when the casein outer layer was gradually degraded by the intestinal protease in the simulated intestine condition. Such unique properties enable maintenance of the bioactivity of the drugs and thus enhance the drug delivery efficiency. *Ex vivo* experiments showed that the LBL CN-DOX-IO improved the translocation of DOX across microvilli and its absorption in the small intestine sacs. In vivo imaging of mice that were orally administered with these LBL CN-ICG-IO nanostructures

further confirmed that the reported drug delivery vehicles could pass the stomach without significant degradation, and then accumulated in the small intestine. In addition, the magnetic iron oxide nanoparticle core offered an MRI contrast enhancing capability for in vivo imaging guided drug delivery [131].

Kossatz S. et al., 2015, fabricated superparamagnetic iron oxide nanoparticles (MF66) were electrostatically functionalized with multivalent pseudopeptide (N6L; MF66-N6L), doxorubicin (DOX; MF66-DOX) or both (MF66-N6LDOX). Their cytotoxic potential was assessed in a breast adenocarcinoma cell line MDA-MB-231. Therapeutic efficacy was analyzed on subcutaneous MDA-MB-231 tumor bearing female athymic nude mice. All nanoparticle variants showed an excellent heating potential around 500 W/g Fe in the alternating magnetic field (AMF, conditions: H = 15.4 kA/m, f = 435 kHz). A gradual inter- and intracellular release of the ligands, and nanoparticle uptake in cells was increased by the N6L functionalization. MF66-DOX and MF66-N6LDOX in combination with hyperthermia were more cytotoxic to breast cancer cells than the respective free ligands. They observed a substantial tumor growth inhibition (to 40% of the initial tumor volume, complete tumor regression in many cases) after intratumoral injection of the nanoparticles *in vivo*. The proliferative activity of the remaining tumor tissue was distinctly reduced. The therapeutic effects of breast cancer magnetic hyperthermia could be strongly enhanced by the combination of MF66 functionalized with N6L and DOX and magnetic hyperthermia. This approach combined two ways of tumor cell killing (magnetic hyperthermia and chemotherapy) and represented a straightforward strategy for translation into the clinical practice when injecting nanoparticles intratumorally [132].

Kempen P.J. et al., 2015 studied nanoparticle which offered ultrasound and MRI signal to guide implantation into the peri-infarct zone and away from the most necrotic tissue. The nanoparticle served as a slow release reservoir of insulin-like growth factor (IGF)—a protein shown to increase cell survival. Mesenchymal stem cells labeled with these nanoparticles had detection limits near 9000 cells with no cytotoxicity at the 250 µg/mL concentration required for labeling. They also studied the degradation of the nanoparticles and showed that they cleared from cells in approximately 3 weeks. The presence of IGF increased cell survival up to 40% ($p<0.05$) versus unlabeled cells under *in vitro* serum-free culture conditions [133].

Ebrahimi E., et al., 2016 proposed delivery of active molecules to the target site in a definite manner to produce the desired effects without disturbing the delicate bio-environment. The Fe_3O_4 magnetic nanoparticles were prepared by chemical precipitation of Fe salts in the ratio of 1:2 under alkaline and inert condition. PLGA-PEG1000 triblock copolymer was synthesized by ring-opening polymerization. The properties of this copolymer were characterized using Fourier transform infrared spectroscopy. In addition, the resulting particles were characterized by X-ray powder diffraction, scanning electron microscopy, and vibrating sample magnetometry. The in vitro doxorubicin (DOX) release profiles were obtained by representing the percentage of DOX release. In this report, they used this new method to fabricate PEGylated PLGA particles, and examined the anticancer agent DOX [134].

Tabatabaei S.N. et al., 2015 entailed the concept of remote control of the permeability of the blood–brain barrier by magnetic heating of nanoparticles. Despite advances in neurology, drug delivery to the brain remains a substantial challenge. This was mainly due to the insurmountable and selective nature of the blood–brain barrier (BBB). In this study, they showed that the thermal energy generated by magnetic heating (hyperthermia) of commercially available magnetic nanoparticles (MNPs) in the brain capillaries of rats transiently increase barrier permeability. Here, the fluorescent Evans Blue (EB) dye was used to verify the BBB integrity. Results indicated a substantial but reversible opening of the BBB where hyperthermia was applied. Also, in this investigation, analysis of CD68 immunoreactivity, an indicator of inflammation, implied that this technique was not associated with any inflammation. They had previously investigated theranostic (therapeutic and diagnostic) capabilities of the MNPs, therefore, the findings presented in investigation were particularly encouraging for a novel targeted drug delivery system to the brain [135].

Patra S. et al 2016 prepared water-soluble superparamgnetic iron oxide nanoparticles (SPIONs) coated with a dual responsive polymer for targeted delivery of anticancer hydrophobic drug (curcumin) and hyperthermia treatment. Herein, superparamagnetic mixed spinel ($MnFe_2O_4$) was used as a core material (15–20 nm) and modified with carboxymethyl cellulose (water-soluble component), folic acid (tagging agent), and dual responsive polymer (poly-N isopropylacrylamide-co-poly glutamic acid) by microwave radiation. Lower critical solution temperature (LCST) of the thermoresponsive copolymer was observed to be around 40 °C,

which is appropriate for drug delivery. The polymer-SPIONs show high drug loading capacity (89%) with efficient and fast drug release at the desired pH (5.5) and temperature (40 °C) conditions. Along with this, the SPIONs showed a very fast increase in temperature (45 °C in 2 min) when interacting with an external magnetic field, which was an effective and appropriate temperature for the localized hyperthermia treatment of cancer cells. The cytocompatibility of the curcumin loaded SPIONs was studied by the methyl thiazol tetrazolium bromide (MTT) assay, and cells were imaged by fluorescence microscopy. To explore the targeting behavior of curcumin loaded SPIONs, a simple magnetic capturing system (simulating a blood vessel) was constructed and it was found that ~99% of the nanoparticle accumulated around the magnet in 2 min by traveling a distance of 30 cm. Along with this, to explore an entirely different aspect of the responsive polymer, its antibacterial activity toward an E. coli strain was also studied. It was found that responsive polymer is not harmful for normal or cancer cells but shows a good antibacterial property [136].

Chowdhuri A.R. et al., 2016 developed a novel multifunctional porous nanoplatform for targeted anticancer drug delivery with cell imaging and magnetic resonance imaging. They developed magnetic nanoscale metal organic frameworks (NMOF) for potential targeted drug delivery. These magnetic NMOFs were fabricated by incorporation of Fe_3O_4 nanoparticles into porous isoreticular metal organic frameworks (IRMOF-3). To achieve targeted drug delivery towards cancer cells specifically, folic acid was conjugated to the NMOF surface. Then, the fluorescent molecule rhodamine B isothiocyanate (RITC) was conjugated to the NMOFs for biological imaging applications. The synthesized magnetic NMOFs were observed to be smaller than 100 nm and were found to be nontoxic towards human cervix adenocarcinoma (HeLa) and murine fibroblast (NIH3T3) cells according to cell viability assays. The cancer chemotherapy drug paclitaxel was conjugated to the magnetic NMOFs through hydrophobic interactions with a relatively high loading capacity. Moreover, these folic acid-conjugated magnetic NMOFs showed stronger T2-weighted MRI contrast towards the cancer cells, justifying their possible significance in imaging [137].

Elbialy N.S. et al., 2015 focused on designing biocompatible magnetic nanoparticles that can be used as a nanocarrier's candidate for MTD regimen. Magnetic gold nanoparticles (MGNPs) were prepared and functionalized with thiol-terminated polyethylene glycol (PEG), then loaded

with anti-cancer drug doxorubicin (DOX). The physical properties of the prepared NPs were characterized using different techniques. Transmission electron microscopy (TEM) revealed the spherical mono-dispersed nature of the prepared MGNPs with size about 22 nm. Energy dispersive X-ray spectroscopy (EDX) assured the existence of both iron and gold elements in the prepared nanoparticles. Fourier transform infrared (FTIR) spectroscopy assessment revealed that PEG and DOX molecules were successfully loaded on the MGNPs surfaces, and the amine group of DOX was the active attachment site to MGNPs. *In vivo* studies proved that magnetic targeted drug delivery could provide a higher accumulation of drug throughout tumor compared with that delivered by passive targeting. This clearly appeared in tumor growth inhibition assessment, biodistribution of DOX in different body organs in addition to the histopathological examinations of treated and untreated Ehrlich carcinoma. To assess the in vivo toxic effect of the prepared formulations, several biochemical parameters such as aspartate aminotransferase (AST), alanine transaminase (ALT), lactate dehydrogenase (LDH), creatine kinase MB (CK-MB), urea, uric acid and creatinine were measured. MTD technology not only minimizes the random distribution of the chemotherapeutic agents, but also reduces their side effects to healthy tissues, which were the two primary concerns in conventional cancer therapies [138].

Qiu X.L. et al., 2015 developed a facile strategy to prepare magnetic nanocarriers where ultrasmall superparamagnetic Fe3O4 nanoparticles were used as the core with mesoporous silica as the shell followed by the covalent installation of a layer of β-cyclodextrins on the outer surfaces. The smart hybrid nanomaterials showed remarkable pH- and sugar-responsive cargo release property and low cytotoxicity as proved by an MTT assay with HEK293T cell lines [139].

Hashemi-Moghaddam H. et al., 2016 synthesized magnetic molecularly imprinted polymer (MIP) using polydopamine. Synthesized MIP was used for controlled 5-fluorouracil (5-FU) delivery in a spontaneous model of breast adenocarcinoma in Balb/c mice in the presence of an external magnetic field. Antitumor effectiveness of 5-FU imprinted polymer (5-FU-IP) was evaluated in terms of tumor-growth delay, tumor-doubling time, inhibition ratio, and histopathology. Results showed higher efficacy of 5-FU-IP in the presence of magnetic field upon suppressing tumor growth than free 5-FU and 5-FU-IP without magnetic field. The 5-FU and Fe distribution among tissues were evaluated by high-performance liquid chromatography

and flame atomic absorption spectrometry, respectively. The obtained results, showed significantly deposition of 5-FU in the 5-FU-IP treated group with magnetic field. Thus, magnetic 5-FU-IP was promising for breast cancer therapy with high efficacy [140].

Zhao J. et al., 2015 fabricated aerogels from polyethylenimine-grafted cellulose nanofibrils (CNFs-PEI) for the first time as a novel drug delivery system. The morphology and structure of the CNFs before and after chemical modification were characterized by scanning electron microscopy (SEM), Fourier transform infrared spectroscopy (FTIR), and X-ray photoelectron spectroscopy (XPS). Water-soluble sodium salicylate (NaSA) was used as a model drug for the investigation of drug loading and release performance. The CNFs-PEI aerogels exhibited a high drug loading capability (287.39 mg/g), and the drug adsorption process could be well described by Langmuir isotherm and pseudo-second-order kinetics models. Drug release experiments demonstrated a sustained and controlled release behavior of the aerogels highly dependent on pH and temperature. This process followed quite well the pseudo-second-order release kinetics. Owing to the unique pH- and temperature-responsiveness together with their excellent biodegradability and biocompatibility, the CNFs-PEI aerogels were very promising as a new generation of controlled drug delivery carriers, offering simple and safe alternatives to the conventional systems from synthetic polymers [141].

Zhang G. et al., 2015 designed pH-responsive nanoplatform, hydroxylated mesoporous nanosilica (HMNS) coated by polyethylenimine (PEI) coupled with gadolinium and folic acid (FA) (Gd-FA-Si), to deliver anticancer drug targeting and to promote contrast effect for tumor cells using magnetic resonance (MR) spectrometer. Doxorubicin (DOX) was chosen as the anticancer drug and loaded into nanopores of HMNS, then its release in simulated body fluid could be controlled through adjusting the pH. This nanoplatform could significantly enhance the MR contrast effect, and the highest theoretical relaxivity per nanoplatform could even be approximately 1.28 × 106 mm–1s–1 because of the high Gd payload (2.61 × 105 per nanoplatform). The entire system possessed a high targeting performance to Hela and MDA-MB-231 cells because the FA located in the system could specifically bind to the folate–receptor sites on the surface of cell. Compared with free DOX, the nanoplatform presented a higher cell inhibition effect on the basis of cell assay. Therefore, this nanoplatform could be potentially applied as a tumor-targeted T1 MR contrast agent and pH-sensitive drug carrier system [142].

Mohammadi M. et al., 2015 used RNA aptamer against EpCAM (EpDT3) attached physically to newly synthesized non-viral vector, based on single-walled carbon nanotube (SWNT) conjugated to piperazine–polyethylenimine derivative. The DNA transfection efficiency and siRNA delivery activity of the synthesized vector was investigated against upregulated BCL9l, which has been associated with breast and colorectal cancers.The complexes of the vector–aptamer/siRNA could specifically induce apoptosis by more than 20% in MCF-7 cell line as a positive EpCAM than MDA-MB-231 cells which are EpCAM negative. The decrease of BCL9l protein level was observed with western blot analysis in MCF-7 cells indicating the targeted silencing activity of the complex [143].

Liu L. et al., 2015 developed an amphiphilic and biodegradable ternary copolymer conjugated with folate as ligand, polyethylenimine-graft-polycaprolactone-block-poly(ethylene glycol)-folate (PEI–PCL–PEG–Fol) and evaluated it for targeted siRNA delivery via folate–FR recognition. The amphiphilic character of similar polymers was shown previously to support endosomal release of endocytosed nanocarriers and to promote formation of long circulating micelles. The obtained PEI–PCL–PEG–Fol exhibited less cytotoxicity in comparison with the corresponding ternary copolymer without folate (PEI–PCL–PEG) and with unmodified PEI25kDa. Stable micelle-like polyplexes with hydrodynamic diameters about 100 nm were found to have a zeta potential of +8.6 mV, which was lower than that of micelleplexes without folate-conjugation (+13–16 mV). Nonetheless, increased cellular uptake and in vitro gene knockdown of PEI–PCL–PEG–Fol/siRNA micelleplexes were observed in SKOV-3 cells, an FR overexpressing cell line, in comparison with the nonfolate-conjugated ones. Moreover, PEI–PCL–PEG–Fol/siRNA micelleplexes exhibited excellent stability in vivo during the analysis of 120 min and a longer circulation half life than hyPEI25kDa/siRNA polyplexes. Most interestingly, the targeted delivery system yielded 17% deposition of the i.v. injected siRNA per gram in the tumor after 24 h due to the effective folate targeting and the prolonged circulation [144].

Taghavi S. et al., 2017 modified branched polyethylenimine (PEI 10 kDa) and grafted it through polyethylene glycol (PEG) linker to carboxylated single-walled carbon nanotubes (SWCNT) to serve as a vehicle for shRNA delivery. The SWNT-PEG-PEI conjugate was covalently attached to AS1411 aptamer as the nucleolin ligand to target the co-delivery system to

the tumor cells overexpressing nucleolin receptors on their surface. The final vehicle was eventually obtained after intercalation of DOX with pBcl-xL shRNA-SWCNT-PEG-10-10%PEI-Apt. Cell viability assay, GFP expression and transfection experiment against L929 (-nucleolin) and AGS (+nucleolin) cells illustrated that the tested targeted delivery system inhibited the growth of nucleolin-abundant gastric cancer cells with strong cell selectivity. Subsequently, they illustrated that the combination treatment of the selected shRNAs and DOX had excellent tumoricidal efficacy as verified by MTT assay. Furthermore, very low concentration of DOX, approximately 58-fold lower than its IC50 concentration, was used which could mitigate toxic side effects of DOX. Overall, the work revealed that combination of shRNA-mediated gene-silencing strategy with chemotherapeutic agents constitutes a valuable and safe approach for antitumor activity [145].

Wang M., et al., 2015 fabricated dual pH-sensitive co-delivery system, programmed to respond to tumor extracellular pH (6.0–7.0) and intracellular pH (4.5–6.5) environments, for the controlled co-delivery of DOX and genes. Tumor intracellular pH-sensitive cationic doxorubicin (DOX)–poly(ethyleneimine) (PEI) conjugates (DOX–PEI, DP) were synthesized via pH-sensitive hydrazone bonds. As O-carboxymethyl-chitosan (CMCS) possesses cationic charges under pH 6.5 and is anionically charged above pH 7.0, tumor extracellular pH (6.0–7.0) triggered charge reversal CMCS–poly(ethylene glycol) (PEG)–aspargine–glycine–arginine (NGR) copolymers (CMCS–PEG–NGR, CPN) were synthesized. The two materials with different properties helped to construct the dual pH-sensitive co-delivery system. First, the cationic DP interacted with anionic pDNA to form a DOX and gene co-loaded DP/pDNA (DPD) core. Then, anionic CPN was adsorbed on the surfaces of the positive charged DPD to form dual pH-sensitive CPN/DPD (CDPD). CDPD and DPD exhibited spherical shapes, uniform particle size distributions (137.4 ± 2.7 nm and 80.0 ± 4.2 nm, respectively), and positive zeta potentials (8.25 mV and 23.59 mV, respectively). Targeted cellular uptakes of CDPD were confirmed (cellular uptakes of CDPD were 92.49 ± 2.28% and 67.82 ± 0.07% in CD13-positive A549 cells and CD13-negative HepG2 cells, respectively). The dissociation of CPN from CDPD at acidic tumor tissue was evaluated (transfection efficiencies of CDPD at pH 7.4 and pH 6.0 were 11.43 ± 0.59% and 20.20 ± 1.21%, respectively). The internalized DPD programmable release of DOX and pDNA was investigated under simulated endosomal conditions. The results suggest that dual

pH-sensitive CDPD was conducive to targeted delivery and the novel functional materials ensured the successful construction of novel dual pH-sensitive CDPD using a simple method [146].

Lo Y. L. et al., 2015 suggested MicroRNA-128 (miR-128) as an attractive therapeutic molecule with powerful glioblastoma regulation properties. However, miR-128 lacked biological stability and leads to poor delivery efficacy in clinical applications. In previous study, they demonstrated two effective transgene carriers, including polyethylenimine (PEI)-decorated superparamagnetic iron oxide nanoparticles (SPIONs) as well as chemically-conjugated chondroitin sulfate-PEI copolymers (CPs). In this report, they optimized conditions for coating CPs onto the surfaces of SPIONs, forming CPIOs, for magneto-gene delivery systems. The optimized weight ratio of the CPs and SPIONs was 2 : 1, which resulted in the formation of a stable particle as a good transgene carrier. The hydrodynamic diameter of the CPIOs is ~136 nm. The gel electrophoresis result demonstrated that the weight ratio of CPIO/DNA required to completely encapsulate pDNA was ≥3. The *in vitro* tests of CPIO/DNA were done in 293 T, CRL5802, and U87-MG cells in the presence and absence of an external magnetic field. The magnetofection efficiency of CPIO/DNA was measured in the three cell lines with or without fetal bovine serum (FBS). CPIO/DNA exhibited remarkably improved gene expression in the presence of the magnetic field and 10% FBS as compared with a gold non-viral standard, PEI/DNA, and a commercial magnetofection reagent, PolyMag/DNA. In addition, CPIO/DNA showed less cytotoxicity than PEI/DNA and PolyMag/DNA against the three cell lines. The transfection efficiency of the magnetoplex improved significantly with an assisted magnetic field. In miR-128 delivery, a microRNA plate array and fluorescence in situ hybridization were used to demonstrate that CPIO/pMIRNA-128 indeed expresses more miR-128 with the assisted magnetic field than without. In a biodistribution test, CPIO/Cy5-DNA showed higher accumulation at the tumor site where an external magnet is placed nearby [147].

Borgheti-Cardoso L.N. et al., 2015 developed and characterized non-viral carriers to deliver siRNA locally, based on polyethylenimine (PEI) as gene carrier, and a self-assembling drug delivery system that forms a gel in situ. Liquid crystalline formulations composed of monoglycerides (MO), PEI, propylene glycol (PG) and 0.1 M Tris buffer pH 6.5 were developed and characterized by polarized light microscopy, Small Angle X-ray Scattering (SAXS), for their

ability to form inverted type liquid crystalline phases (LC2) in contact with excess water, water absorption capacity, ability to complex with siRNA and siRNA release. In addition, gel formation in vivo was determined by subcutaneous injection of the formulations in mice. In excess water, precursor fluid formulation rapidly transforms into a viscous liquid crystalline phase. The presence of PEI influenced the liquid crystalline structure of the LC2 formed and was crucial for complexing siRNA. The siRNA was released from the crystalline phase complexed with PEI. The release rate was dependent on the rate of water uptake. The formulation containing MO/PEI/PG/Tris buffer at 7.85:0.65:76.5:15 (w/w/w/w) complexed with 10 μM of siRNA, characterized as a mixture of cubic phase (diamond-type) and inverted hexagonal phase (after contact with excess water), showed sustained release for 7 days *in vitro*. In mice, *in situ* gel formation occurred after subcutaneous injection of the formulations, and the gels were degraded in 30 days. Initially a mild inflammatory process occurred in the tissue surrounding the gel; but after 14 days the tissue appeared normal. Taken together, this work demonstrated the rational development of an in situ gelling formulation for local release of siRNA [148].

Li J.M. et al., 2015 developed a simple multifunctional nanocarrier based on polyethylenimine (PEI) to codeliver doxorubicin (DOX) and BCL2 small interfering RNA (siRNA) for overcoming multidrug resistance (MDR) and enhancing apoptosis in MCF-7/Adr cancer cells by combining chemotherapy and RNA interference (RNAi) therapy. The low-molecular-weight branch PEI was used to conjugate hydroxypropyl-β-cyclodextrin (HP-β-CD) and folic acid (FA), forming the codelivery nanocarrier (FA-HP-β-CD-PEI) to encapsulate DOX with the cavity HP-β-CD and bind siRNA with the positive charge of PEI for tumor-targeting codelivering drugs. The drug-loaded nanocomplexes (FA-HP-β-CD-PEI/DOX/siRNA) showed uniform size distribution, high cellular uptake, and significant gene suppression of BCL2, displaying the potential of overcoming MDR for enhancing the effect of anticancer drugs. Furthermore, the nanocomplexes achieved significant cell apoptosis through a mechanism of downregulating the antiapoptotic protein BCL2, resulted in improving therapeutic efficacy of the coadministered DOX by tumor targeting and RNA interference. The study indicated that combined RNAi therapy and chemotherapy using our functional co-delivery nanocarrier could overcome MDR and enhance apoptosis in MDR cancer cells for a potential application in treating MDR cancers [149].

Yang G. et al., 2015 developed WS2 nanosheets with their surface pre-adsorbed with iron oxide (IO) nanoparticles via self-assembly coated with a mesoporous silica shell, on to which polyethylene glycol (PEG) was attached as theranostic platform for cancer therapy. The obtained WS2-IO@MS-PEG composite nanoparticles exhibited many interesting inherent physical properties, including high near-infrared (NIR) light and X-ray absorbance, as well as strong superparamagnetism. In the mean time, the mesoporous silica shell in WS2-IO@MS-PEG could be loaded with a chemotherapy drug, doxorubicin (DOX), whose intracellular release afterwards may be triggered by NIR-induced photothermal heating for enhanced cancer cell killing. Upon systemic administration of such drug-loaded nano-theranostics, efficient tumor homing of WS2-IO@MS-PEG/DOX is observed in tumor-bearing mice as revealed by three-modal fluorescence, magnetic resonance (MR), and X-ray computed tomography (CT) imaging. In vivo combined photothermal & chemotherapy is then carried out with WS2-IO@MS-PEG/DOX, achieving a remarkably synergistic therapeutic effect superior to the respective mono-therapies. The study highlighted the promise of developing multifunctional nanoscale theranostics based on two-dimensional transition metal dichalcogenides (TMDCs) such as WS2 for multimodal imaging-guided combination therapy of cancer [150].

Das M. et al., 2015 investigated the theranostic capabilities of nutlin-3a loaded poly (lactide-co-glycolide) nanoparticles, functionalized with a targeting ligand (EpCAM aptamer) and an imaging agent (quantum dots) for cancer therapy and bioimaging. A wide spectrum of in vitro analysis (cellular uptake study, cytotoxicity assay, cell cycle and apoptosis analysis, apoptosis associated proteins study) revealed superior therapeutic potentiality of targeted NPs over other formulations in EpCAM expressing cells. Moreover, developed nanotheranostic system served as a superlative bio-imaging modality both in 2D monolayer culture and tumor spheroid model. The result suggested that, these aptamer-guided multifunctional NPs may act as indispensable nanotheranostic approach toward cancer therapy [151].

Tian G. et al., 2015 overviewed multi-drug resistance (MDR) as a major cause of failure in cancer chemotherapy. Tocopheryl polyethylene glycol 1000 succinate (TPGS) has been extensively investigated for overcoming MDR in cancer therapy because of its ability to inhibit P-glycoprotein (P-gp). In this work, TPGS was for the first time used as a new surface modifier to functionalize NaYbF4:Er upconversion nanoparticles (UNCPs) and endowed the as-prepared

products (TPGS-UCNPs) with excellent water-solubility, P-gp inhibition capability and imaging-guided drug delivery property. After the chemotherapeutic drug (doxorubicin, DOX) loading, the as-formed composites (TPGS-UCNPs-DOX) exhibited potent killing ability for DOX-resistant MCF-7 cells. Flow-cytometric assessment and Western blot assay showed that the TPGS-UCNPs could potently decrease the P-gp expression and facilitate the intracellular drug accumulation, thus achieving MDR reversal. Moreover, considering that UCNPs process efficient upconversion emission and Yb element contained in UCNPs has strong X-ray attenuation ability, the as-obtained composite could also serve as a dual-modal probe for upconversion luminescence (UCL) imaging and X-ray computed tomography (CT) imaging, making them promising for imaging-guided cancer therapy [152].

Kang T. et al., 2017 reviewed magnetic nanoparticles (MNPs) for their potential applications to cancer diagnosis and treatment. As a viable solution to obstacles, advances in nanoparticle surface engineering augmented by a profound understanding of cancer physiology presented new opportunities for MNP-based imaging and therapeutic agents. Stimuli-responsive ligands, rationally designed to interact with various physicochemical aspects, could improve the performance of MNPs in cancer-targeted imaging and therapy. In this review, they highlighted recent progress in the design of MNP-based stimuli-responsive nanomaterials and their applications to cancer diagnosis and treatment [153].

Patitsa M. et al., using *in silico*, *in vitro* and *in vivo* studies, showed for the first time that magnetic nanoparticles coated with polyarabic acid have superior imaging, therapeutic, and biocompatibility properties. They demonstrated that polyarabic acid coating allows for efficient penetration of cell membranes and internalization into breast cancer cells. Polyarabic acid also allows reversible loading of the chemotherapeutic drug Doxorubicin, which upon release suppresses tumor growth *in vivo* in a mouse model of breast cancer. Furthermore, these nanomaterials provide *in vivo* contrasting properties, which directly compare with commercial gadolinium-based contrasting agents. Finally, they reported excellent biocompatibility, as these nanomaterial cause minimal, if any cytotoxicity in vitro and in vivo. They thus proposed that magnetic nanodevices coated with polyarabic acid offer a new avenue for theranostics efforts as efficient drug carriers, while providing excellent contrasting properties due to their ferrous

magnetic core, which can help the future design of nanomaterials for cancer imaging and therapy [154].

Chen H. et al., 2017 studied use of X-ray as the irradiation source; a photodynamic therapy process can be initiated from under deep tissues. This technology, referred to as X-ray induced PDT, or X-PDT, holds great potential to treat tumors at internal organs. To this end, one question is how to navigate the treatment to tumors with accuracy with external irradiation. They addressed the issue with a novel, LiGa5O8: Cr (LGO:Cr)-based nanoscintillator, which emits persistent, near-infrared X-ray luminescence. This permits deep-tissue optical imaging that can be employed to guide irradiation. Specifically, we encapsulated LGO:Cr nanoparticles and a photosensitizer, 2,3-naphthalocyanine, into mesoporous silica nanoparticles. The nanoparticles were conjugated with cetuximab and systemically injected into H1299 orthotopic non-small cell lung cancer tumor models. The nanoconjugates can efficiently home to tumors in the lung, confirmed by monitoring X-ray luminescence from LGO:Cr. Guided by the imaging, external irradiation was applied, leading to efficient tumor suppression while minimally affecting normal tissues. The present study was the first to demonstrate, with systematically injected nanoparticles, that X-PDT can suppress growth of deep-seated tumors. The imaging guidance was also new to X-PDT, and is significant to the further transformation of the technology [155].

Alberti D. et al., 2017 studied combination of different therapeutic modalities as a promising option to combat the recurrence of tumors. In this study, polylactic and polyglycolic acid nanoparticles were used for the simultaneous delivery of a boron–curcumin complex (RbCur) and an amphiphilic gadolinium complex into tumor cells with the aim of performing boron and gadolinium neutron capture therapy (NCT) in conjunction with the additional antiproliferative effects of curcumin. Furthermore, the use of Gd complexes allowed magnetic resonance imaging (MRI) assessment of the amount of B and Gd internalized by tumor cells. Poly(lactic-co-glycolic acid) (PLGA) nanoparticles were targeted to ovarian cancer (IGROV-1) cells through folate receptors, by including in the formulation a PEGylated phospholipid functionalized with the folate moiety. NCT was performed on IGROV-1 cells internalizing 6.4 and 78.6 $\mu g\, g^{-1}$ of 10B and 157Gd, respectively. The synergic action of neutron treatment and curcumin cytotoxicity was shown to result in a significant therapeutic improvement [156].

Nagesetti A. et al., 2017 grafted pegylated multifunctional probe of Ormosil nanoparticles (PEGCDSIR820) loaded with Near Infrared dye (NIR; IR820) and a chemotherapeutic drug, Doxorubicin (DOX) for cancer theranostic applications. PEGCDSIR820 nanoparticles had an average diameter of 58.2 ± 3.1 nm, zeta potential of − 6.9 ± 0.1 mV in cell culture media and stability against aggregation in physiological buffers. The encapsulation efficiency of DOX was 65.0 ± 3.0%, and that of IR820 was 76.0 ± 2.1%. PEGCDSIR820 showed no cytotoxicity in ovarian cancer cells (Skov-3). The cytotoxicity markedly increased when Skov-3 cells incubated with PEGCDSIR820 particles were exposed to 808 nm laser due to the combination of adjuvant hyperthermia (43 °C) and enhanced DOX release. Exposure to laser enhanced the release of DOX, 45% of DOX release was observed in 3 h compared to 23% without laser exposure. Confocal imaging in Skov-3 cells showed that the combination of hyperthermia due to NIR exposure and release of DOX caused cell necrosis. Furthermore, in spheroids exposed to NIR laser penetration of DOX was deeper compared to the absence of laser exposure. Skov-3 spheroids incubated with pegylated nanoparticles for 24 h and exposed to laser showed 94% reduction in cell viability. Encapsulation of IR820 in PEGCDSIR820 increased the *in-vivo* elimination half-life to 41.0 ± 7.2 h from 30.5 ± 0.5 h of free IR820 [157].

Mohammad F. and Al-Lohedan H.A. 2017 developed superparamagnetic iron oxide nanoparticles (SPIONs) to be appropriate for the diagnosis and treatment of cancer cells by means of magnetic resonance imaging (MRI) and magnetically controlled hyperthermia/drug delivery (respectively). For the preparation of composite, they started with SPIONs, followed by its coating with gold to form SPIONs@Au, which further conjugated with luteinizing hormone-releasing hormone (LHRH) protein by making use of the cysteamine (Cyst) space linker and finally loaded with 5-Fluororacil (5-Fu) anticancer drug to form SPIONs@Au-Cyst-LHRH_5-Fu composite. The SQUID magnetic studies provided the information for the superparamagnetic behavior of the drug loaded SPIONs and the saturation magnetization (Ms) values observed to be about 11 emu/g and the blocking temperature (TB) of 348 K. On testing the particles to see the effects of magnetic fluid hyperthermia (MFH) due to some changes in the solvent medium and oscillating frequency, the material seemed to be highly active in aqueous medium and the activity increased with respect to the applied frequency of oscillation (430 Hz > 230 Hz > 44 Hz). From the heat release studies, the calculated specific power loss (SPL) values for the

SPIONs@Au-Cyst-LHRH_5-Fu composite were at the highest of 1068 W/g in water (430 Hz) vs the least of 68 W/g in toluene (44 Hz). Further, the drug release studies tested under the influence of magnetic field provided the information that the composite released its entire loaded drug following an exposure to the magnetic field (430 Hz over 4 h time), while only 53% (over 5 h) for the controlled measurements of no magnetic field, thereby supporting to have the magnetic field so as to observe the externally controlled drug release effects. Finally, the results of the study provide the information that the SPIONs@Au-Cyst-LHRH_5-Fu composite can be potential for theranostic applications of cancer through the phenomenon of applying for MRI, magnetically controlled hyperthermia and drug delivery externally [158].

Gao N. et al., 2017 studied obstacles in intraperitoneal (i.p.) chemotherapy of peritoneal tumors. Targeted theranostic nanoparticles offered an opportunity to enhance the efficacy of i.p. therapy by increasing intratumoral drug delivery to overcome resistance, mediating image-guided drug delivery, and reducing systemic toxicity. Herein they reported that i.p. delivery of urokinase plasminogen activator receptor (uPAR) targeted magnetic iron oxide nanoparticles (IONPs) led to intratumoral accumulation of 17% of total injected nanoparticles in an orthotopic mouse pancreatic cancer model, which was three-fold higher compared with intravenous delivery. Targeted delivery of near infrared dye labeled IONPs into orthotopic tumors could be detected by non-invasive optical and magnetic resonance imaging. Histological analysis revealed that a high level of uPAR targeted, PEGylated IONPs efficiently penetrated into both the peripheral and central tumor areas in the primary tumor as well as peritoneal metastatic tumor. Improved theranostic IONP delivery into the tumor center was not mediated by nonspecific macrophage uptake and was independent from tumor blood vessel locations. Importantly, i.p. delivery of uPAR targeted theranostic IONPs carrying chemotherapeutics, cisplatin or doxorubicin, significantly inhibited the growth of pancreatic tumors without apparent systemic toxicity. The levels of proliferating tumor cells and tumor vessels in tumors treated with the above theranostic IONPs were also markedly decreased. The detection of strong optical signals in residual tumors following i.p. therapy suggested the feasibility of image-guided surgery to remove drug-resistant tumors. Therefore, results supported the translational development of i.p. delivery of uPAR-targeted theranostic IONPs for image-guided treatment of peritoneal tumors [159].

Wang Z. et al., 2017 reported the development of an active targeting nano-sized theranostic superparamagnetic iron oxide (SPIO) platform for significantly increasing the imaging sensitivity and energy deposition efficiency using a clinical MRgFUS system. The surfaces of these PEGylated SPIO nanoparticles (NPs) were decorated with anti-EGFR (epidermal growth factor receptor) monoclonal antibodies (mAb) for targeted delivery to lung cancer with EGFR overexpression. The potential of these targeted nano-theranostic agents for MRI and MRgFUS ablation was evaluated *in vitro* and *in vivo* in a rat xenograft model of human lung cancer (H460). Compared with nontargeting PEGylated SPIO NPs, the anti-EGFR mAb targeted PEGylated SPIO NPs demonstrated better targeting capability to H460 tumor cells and greatly improved the MRI contrast at the tumor site. Meanwhile, this study showed that the targeting NPs, as synergistic agents, could significantly enhance the efficiency for in vivo ultrasonic energy deposition in MRgFUS. Moreover, they demonstrated that a series of MR methods including T2-weighted image (T2WI), T1-weighted image (T1WI), diffusion-weighted imaging (DWI) and contrast-enhanced T1WI imaging, could be utilized to noninvasively and conveniently monitor the therapeutic efficacy in rat models by MRgFUS [160].

Chi Y. H. et al., 2017 aimed to identify targeting peptides with diagnostic and therapeutic utility that possess broad subtype specificity for SCLC and non-small cell lung cancer (NSCLC). They performed phage display biopanning of H460 LCC cells to select broad-spectrum lung cancer-binding peptides, since LCC has recently been categorized as an undifferentiated tumor type within other histological subcategories of lung cancer. Three targeting phages (HPC1, HPC2, and HPC4) and their respective displayed peptides (HSP1, HSP2, and HSP4) were able to bind to both SCLC and NSCLC cell lines, as well as clinical specimens, but not to normal pneumonic tissues. In vivo optical imaging of phage homing and magnetic resonance imaging (MRI) of peptide-SPIONs revealed that HSP1 was the most favorable probe for multimodal molecular imaging. Using HSP1-SPION, the T2-weighted MR signal of H460 xenografts was decreased up to 42%. In contrast to the tight binding of HSP1 to cancer cell surfaces, HSP4 was preferentially endocytosed and intracellular drug delivery was thereby effected, significantly improving the therapeutic index of liposomal drug in vivo. Liposomal doxorubicin (LD) conjugated to HSP1, HSP2, or HSP4 had significantly greater therapeutic efficacy than non-targeting liposomal drugs in NSCLC (H460 and H1993) animal models. Combined therapy with

an HSP4-conjugated stable formulation of liposomal vinorelbine (sLV) further improved median overall survival (131 vs. 84 days; P = 0.0248), even in aggressive A549 orthotopic models. Overall, these peptides have the potential to guide a wide variety of tailored theranostic agents for targeting therapeutics, non-invasive imaging, or clinical detection of SCLC and NSCLC [161].

Lu z., et al., 2017 developed multifunctional theranostic nanoplatforms for targeted cancer imaging and therapy. Herein, they explored a general method to prepare mPEG-dBSA-Cy5.5 nanoparticles as a biodegradable agent for tumor imaging and anticancer drug delivery. The functional denatured bovine serum albumin (dBSA) endows this nanoagent with the outstanding physiological stability, biocompatibility and drug loading capacity, while a near-infrared fluorescent (NIRF) dye Cy5.5 allows real-time biophotonic imaging of malignant cancer foci. The obtained mPEG-dBSA-Cy5.5 showed excellent dispersibility and stability in physiological solution, as well as negligible toxicity in vitro. The confocal images demonstrated that mPEG-dBSA-Cy5.5 had good uptake by tumor cells, no matter before or after loading doxorubicin (DOX). Furthermore, DOX released from mPEG-dBSA-Cy5.5/DOX exhibited a typical pH-dependent hallmark, and the cell experiments indicated that the mPEG-dBSA-Cy5.5/DOX have excellent therapeutic efficiency. Overall, the prepared mPEG-dBSA-Cy5.5 may hold a great promise to provide a theranostic nanoplatform for targeted imaging and therapy of cancer [162].

Chen L., et al., 2017 constructed safe and stable theranostics which was beneficial for simultaneous cancer diagnosis and treatment. In this study, bovine serum albumin–gadolinium (BSA–Gd) complexes and MoS2 nanoflakes (MoS2–Gd–BSA) were successfully used as cancer theranostics for dual-modality magnetic resonance (MR)/photoacoustic (PA) imaging and photothermal therapy (PTT). BSA–Gd complexes were prepared by the biomineralization method and then conjugated with MoS2 nanoflakes via an amide bond. The as-prepared MoS2–Gd–BSA possessed a good photostability and photothermal effect. The cytotoxicity assessment and hemolysis assay suggested the excellent biocompatibility of MoS2–Gd–BSA. Meanwhile, MoS2–Gd–BSA could not only achieve in vivo MR/PA dual-modality imaging of xenograft tumors, but also effectively kill cancer cells in vitro and ablate the xenograft tumors in vivo upon 808 nm laser illumination. The biodistribution and histological evaluations indicated the

negligible toxicity of MoS2–Gd–BSA both in vitro and in vivo. Thus, results substantiated the potential of MoS2–Gd–BSA for cancer theranostics [163].

Zhang S. et al., 2017 demonstrated a terrylenediimide (TDI)-poly(acrylic acid) (TPA)-based nanomedicine (TNM) platform used as an intrinsic theranostic agent. As an exploratory paradigm in seeking biomedical applications, TDI was modified with poly(acrylic acid)s (PAAs), resulting in eight-armed, star-like TPAs composed of an outside hydrophilic PAA corona and an inner hydrophobic TDI core. TNMs were readily fabricated via spontaneous self-assembly. Without additional vehicle and cargo, the as-prepared TNMs possessed a robust nanostructure and high photothermal conversion efficiency up to approximately 41%. The intrinsic theranostic properties of TNMs for use in photoacoustic (PA) imaging by a multispectral optoacoustic tomography system and in mediating photoinduced tumor ablation were intensely explored. Result suggested that the TNMs could be successfully exploited as intrinsic theranostic agents for PA imaging-guided efficient tumor PTT. Thus, these TNMs hold great potential for (pre)clinical translational development [164].

Chen J. et al., 2017 reported theranostic polymer microcapsules composed of hydrogen-bonded multilayers of tannic acid and poly(N-vinylpyrrolidone) that produced high imaging contrast and delivered the anticancer drug doxorubicin upon low-power diagnostic or high-power therapeutic ultrasound irradiation. These capsules exhibited excellent imaging contrast in both brightness and harmonic modes and show prolonged contrast over six months, unlike commercially available microbubbles. They also demonstrated low-dose gradual and high-dose fast release of doxorubicin from the capsules by diagnostic (∼100 mW/cm2) and therapeutic (>10 W/cm2) ultrasound irradiation, respectively. They showed that the imaging contrast of the capsules can be controlled by varying the number of layers, polymer type (relatively rigid tannic acid versus more flexible poly(methacrylic acid)), and polymer molecular weight. *In vitro* study demonstrated that 50% doxorubicin release from ultrasound-treated capsules induced 97% cytotoxicity to MCF-7 human cancer cells, while no cytotoxicity was found without the treatment. Considering the strong ultrasound imaging contrast, high encapsulation efficiency, biocompatibility, and tunable drug release, these microcapsules can be used as theranostic agents for ultrasound-guided chemotherapy [165].

References

1. V. Mohanraj, Y. Chen. Nanoparticles-a review. Tropical Journal of Pharmaceutical Research. 2006, 5(1),561-73.
2. A.Z. Wilczewska, K. Niemirowicz, K.H. Markiewicz, H. Car. Nanoparticles as drug delivery systems. Pharmacological Reports. 2012, 64 (5), 1020-1037.
3. S.R. Mudshinge, A.B. Deore, S. Patil, C.M. Bhalgat. Nanoparticles: emerging carriers for drug delivery. Saudi pharmaceutical journal. 2011, 19(3), 129-141.
4. W.H. De Jong, P.J. Borm. Drug delivery and nanoparticles: applications and hazards. International Journal of Nanomedicine. 2008, 3(2), 133-149.
5. K.T. Nguyen. Targeted nanoparticles for cancer therapy: promises and challenge. Journal of Nanomedicine and Nanotechnology. 2011, 2(5) 1000103e, 1-2.
6. T. Sun, Y.S. Zhang, B. Pang, D.C. Hyun, M. Yang, Y. Xia. Engineered nanoparticles for drug delivery in cancer therapy. Angewandte Chemie International Edition. 2014, 53(46), 12320-12364
7. World Health Organization: http://www.who.int/cancer/en/Leukaemia and Lymphoma Society : https://www.lls.org/lymphom
8. National Cancer Institute: https://www.cancer.gov/types/lymphoma.
9. P. Jares, D. Colomer, E. Campo. Genetic and molecular pathogenesis of mantle cell lymphoma: perspectives for new targeted therapeutics. Nature Reviews Cancer. 2007, 7(10), 750-762.
10. S.J. Corey, M.D. Minden, D.L. Barber, H. Kantarjian, J.C. Wang, A.D. Schimmer. Myelodysplastic syndromes: the complexity of stem-cell diseases. Nature Reviews Cancer. 2007, 7(2), 118-129.
11. T. Hideshima, C. Mitsiades, G. Tonon, P.G. Richardson, K.C. Anderson. Understanding multiple myeloma pathogenesis in the bone marrow to identify new therapeutic targets. Nature Reviews Cancer. 2007, 7(8), 585-598.
12. Lymphoma Research Foundation: http://www.lymphomafacts.org/site/c.gtJSJbMUIuE/b.1268805/k.16F1/Lymphoma_Treatments.htm#lymphoma_treatments.

13. American Cancer Society: https://www.cancer.org/cancer/nonhodgkinlymphoma/treating/chemotherapy.html.
14. B. Seyfarth, A. Josting, M. Dreyling, N. Schmitz. Relapse in common lymphoma subtypes: salvage treatment options for follicular lymphoma, diffuse large cell lymphoma and Hodgkin disease. British Journal of Haematology. 2006, 133(1), 3-18.
15. Cancer.Net, http://www.cancer.net/cancer-types/lymphoma-non-hodgkin/diagnosis
16. USFDA : www.fda.gov/Drugs/DrugSafety/ucm109337.htm
17. USFDA : www.fda.gov/AboutFDA/CentersOffices/.../CDER/ucm095626.htm
18. USFDA :https://www.accessdata.fda.gov/drugsatfda_docs/label/2017/021880s049lbl.pdf
19. C. Pawlyn, M.S. Khan, A. Muls, P. Sriskandarajah, M.F. Kaiser, F.E. Davies, et al. Lenalidomide-induced diarrhea in patients with myeloma is caused by bile acid malabsorption that responds to treatment. Blood. 2014, 124(15), 2467-2468.
20. J.-X. Song, Y. Yan, J. Yao, J.-M. Chen, T.-B. Lu. Improving the solubility of lenalidomide via cocrystals. Crystal Growth & Design. 2014, 14(6), 3069-3077.
21. J.-X. Song, J.-M. Chen, T.-B. Lu. Lenalidomide–Gallic Acid Co-crystals with Constant High Solubility. Crystal Growth & Design. 2015, 15(10), 4869-4875.
22. T. Gomathi, C. Govindarajan, P. Sudha, P.M. Imran, J. Venkatesan, et al. Studies on drug-polymer interaction, in vitro release and cytotoxicity from chitosan particles excipient. International Journal of Pharmaceutics. 2014, 468(1), 214-222.
23. C. M. Hu, S. Aryal, L. Zhang, Nanoparticle-assisted combination therapies for effective cancer treatment. Therapeutic Delivery. 2010, 1(2), 323-334.
24. P. D. Acton, H. F. Kung, Small animal imaging with high resolution single photon emission tomography. Nuclear Medicine and Biology. 2003, 30(8), 889-895.
25. R. Mansi, X. Wang, F. Forrer, S. Kneifel, M. L. Tamma, B. Waser, R. Cescato, J. C. Reubi, H. R. Maecke, Evaluation of a 1, 4, 7, 10-Tetraazacyclododecane-1, 4, 7, 10-Tetraacetic acid–conjugated bombesin-based radioantagonist for the labeling with single-photon emission computed tomography, positron emission tomography, and therapeutic radionuclides. Clinical Cancer Research. 2009, 15(16), 5240-5249.
26. R. Haubner, H. J. Wester, W. A. Weber, C. Mang, S. I. Ziegler, S. L. Goodman, R. Senekowitsch-Schmidtke, H. Kessler, M. Schwaiger, Noninvasive imaging of αvβ3

integrin expression using 18F-labeled RGD-containing glycopeptide and positron emission tomography. Cancer Research. 2001, 61(5), 1781-1785.

27. J. Knuuti, F. M. Bengel, Positron emission tomography and molecular imaging. Heart. 2008, 94(3), 360-367.
28. K. Chen, Z. B. Li, H. Wang, W. Cai, X. Chen, Dual-modality optical and positron emission tomography imaging of vascular endothelial growth factor receptor on tumor vasculature using quantum dots. European Journal of Nuclear Medicine and Molecular Imaging. 2008, 35(12), 2235-2244.
29. S. M. Knowles, A. M. Wu, Advances in immuno–positron emission tomography: antibodies for molecular imaging in oncology, Journal of Clinical Oncology. 2012, 30(31), 3884-3892.
30. R. Hong, N. O. Fischer, T. Emrick, V. M. Rotello, Surface PEGylation and ligand exchange chemistry of FePt nanoparticles for biological applications. Chemistry of Materials. 2005, 17(18), 4617-4621.
31. H. Gu, Z. Yang, J. Gao, C. K. Chang, B. Xu, Heterodimers of nanoparticles: formation at a liquid− liquid interface and particle-specific surface modification by functional molecules. Journal of the American Chemical Society. 2005, 127(1), 34-55.
32. C. Xu, K. Xu, H. Gu, et al., Dopamine as a robust anchor to immobilize functional molecules on the iron oxide shell of magnetic nanoparticles. Journal of the American Chemical Society. 2004, 126(32), 9938-9939.
33. S .W. Chou, Y. H. Shau, P. C. Wu, Y. S. Yang, D. B. Shieh, In vitro and in vivo studies of FePt nanoparticles for dual modal CT/MRI molecular imaging. Journal of the American Chemical Society. 2010, 132(38), 13270-13278.
34. H. Gu, K. Xu, C. Xu, B. Xu, Biofunctional magnetic nanoparticles for protein separation and pathogen detection. Chemical Communications. 2006, 9, 941-949.
35. J. Yao, M. Yang, Y. Duan, Chemistry, biology, and medicine of fluorescent nanomaterials and related systems: new insights into biosensing, bioimaging, genomics, diagnostics, and therapy. Chemical Reviews. 2014, 114(12), 6130-6178.
36. N. Lee, D. Yoo, D. Ling, M. H. Cho, T. Hyeon, J. Cheon, Iron oxide based nanoparticles for multimodal imaging and magneto-responsive therapy. Chemical Reviews. 2015, 115(19), 10637-10689.

37. H. Chen, Z. Zhen, T. Todd, P. K. Chu, J. Xie, Nanoparticles for improving cancer diagnosis. Materials Science and Engineering: R: Reports. 2013, 74(3), 35-69.
38. Q. Wang, L. Lv, Z. Ling, et al., Long-Circulating Iodinated Albumin–Gadolinium Nanoparticles as Enhanced Magnetic Resonance and Computed Tomography Imaging Probes for Osteosarcoma Visualization. Analytical Chemistry. 2015, 87(8), 4299-4304.
39. J. T. Song, X. Q. Yang, X.S. Zhang, D. M. Yan, Z. Y. Wang, Y. D. Zhao, Facile synthesis of gold nanospheres modified by positively charged mesoporous silica, loaded with near-infrared fluorescent dye, for in vivo X-ray computed tomography and fluorescence dual mode imaging. ACS Applied Materials & Interfaces. 2015, 7(31), 17287-17297.
40. G. M. Hahn, Potential for therapy of drugs and hyperthermia. Cancer Research. 1979, 39, 2264-2268.
41. H. H. Kampinga, Cell biological effects of hyperthermia alone or combined with radiation or drugs: a short introduction to newcomers in the field. International Journal of Hyperthermia. 2006, 22(3), 191-196.
42. M. Johannsen, U. Gneveckow, L. Eckelt, et al., Clinical hyperthermia of prostate cancer using magnetic nanoparticles: presentation of a new interstitial technique. International Journal of Hyperthermia. 2005, 21(7), 637-647.
43. Y. Cheng, R. A. Morshed, B. Auffinger, A. L. Tobias, M. S. Lesniak, Multifunctional nanoparticles for brain tumor imaging and therapy. Advanced Drug Delivery Reviews. 2014, 66, 42-57.
44. R. A. Sperling, W.J. Parak, Surface modification, functionalization and bioconjugation of colloidal inorganic nanoparticles. Philosophical Transactions of the Royal Society of London A: Mathematical, Physical and Engineering Sciences. 2010, 368(1915), 1333-1383.
45. F. Sonvico, S. Mornet, S. Vasseur, et al., Folate-conjugated iron oxide nanoparticles for solid tumor targeting as potential specific magnetic hyperthermia mediators: synthesis, physicochemical characterization, and in vitro experiments. Bioconjugate Chemistry. 2005, 16(5), 1181-1188.
46. S. Mornet, S. Vasseur, F. Grasset, E. Duguet, Magnetic nanoparticle design for medical diagnosis and therapy. Journal of Materials Chemistry. 2004, 14(14), 2161-2175.

47. F. M. Kievit, M. Zhang, Surface engineering of iron oxide nanoparticles for targeted cancer therapy, Accounts of Chemical Research. 2011, 44(10), 853-862.
48. Y.Cheng, R. A. Morshed,B. Auffinger, A. L. Tobias, M. S. Lesniak, Multifunctional nanoparticles for brain tumor imaging and therapy. Advanced Drug Delivery Reviews, 2014, 66, 42-57.
49. P. Wust P, U. Gneveckow, P. Wust, et al., Magnetic nanoparticles for interstitial thermotherapy–feasibility, tolerance and achieved temperatures. International Journal of Hyperthermia. 2006, 22(8), 673-85.
50. M. L. Wegscheid, R. A. Morshed, Y. Cheng, M. S. Lesniak, The art of attraction: applications of multifunctional magnetic nanomaterials for malignant glioma, Expert Opinion on Drug Delivery. 2014, 11(6), 957-975.
51. C. S. Kumar, F. Mohammad, Magnetic nanomaterials for hyperthermia-based therapy and controlled drug delivery, Advanced Drug Delivery Reviews. 2011, 63(9), 789-808.
52. S. H. Noh, S. H. Moon, T. H. Shin, Y. Lim, J. Cheon, Recent advances of magneto-thermal capabilities of nanoparticles: From design principles to biomedical applications. Nano Today. 2017, In Press.
53. C. Xu, Z. Yuan, N. Kohler, J. Kim, M. A. Chung, S. Sun, FePt nanoparticles as an Fe reservoir for controlled Fe release and tumor inhibition, Journal of the American Chemical Society. 2009, 131(42), 15346-15351.
54. N. K. Sahu, J. Gupta, D. Bahadur, PEGylated FePt–Fe 3 O 4 composite nano assemblies (CNAs): in vitro hyperthermia, drug delivery and generation of reactive oxygen species (ROS). Dalton Transactions. 2015, 44(19), 9103-9113.
55. E. Ju, Z. Liu, Y. Du, Y. Tao, J. Ren, X. Qu, Heterogeneous assembled nanocomplexes for ratiometric detection of highly reactive oxygen species in vitro and in vivo. ACS Nano. 2014, 8(6), 6014-6023.
56. J. Gallo, N. J. Long, E. O. Aboagye, Magnetic nanoparticles as contrast agents in the diagnosis and treatment of cancer. Chemical Society Reviews. 2013, 42(19), 7816-33.
57. Y. Zheng, Y. Tang, Z. Bao, H. Wang, F. Ren, M. Guo, et al. FePt nanoparticles as a potential X-ray activated chemotherapy agent for hela cells. International Journal of Nanomedicine. 2015, 10, 6435-6444.

58. H.L. Nguyen, L.E. Howard, G.W. Stinton, S.R. Giblin, B.K. Tanner, I. Terry, et al. Synthesis of size-controlled fcc and fct FePt nanoparticles. Chemistry of Materials. 2006, 18(26), 6414-6424.
59. D.E. Laughlin, K. Srinivasan, M. Tanase, L. Wang. Crystallographic aspects of L1 0 magnetic materials. Scripta Materialia. 2005, 53(4), 383-388.
60. X. Hu. Synthesis and characterization of magnetically hard Fe-Pt alloy nanoparticles and nano-islands: University of Delaware; 2016. http://udspace.udel.edu/handle/19716/17738
61. X. DONGBIN. Investigations of doped l10 FePt films for heat assisted magnetic recording (HAMR) 2013. http://scholarbank.nus.edu.sg/bitstream/handle/10635/47547/XuDB.pdf?sequence=1
62. V. Nandwana. Synthesis, characterization and potential applications of iron-platinum nanoparticles: The University of Texas at Arlington, 2009. https://www.academia.edu/2788445/Synthesis_Characterization_And_Potential_Applications_Of_Fept_Nanoparticles
63. T. Burkert, O. Eriksson, S.I. Simak, A.V. Ruban, B. Sanyal, L. Nordström, et al. Magnetic anisotropy of L 1 0 FePt and Fe 1− x Mn x Pt. Physical Review B. 2005,71(13), 134411-134418.
64. F. Wilhelm, P. Poulopoulos, H. Wende, A. Scherz, K. Baberschke, M. Angelakeris, et al. Systematics of the Induced Magnetic Moments in 5 d Layers and the Violation of the Third Hund's Rule. Physical Review Letters. 2001, 87(20), 207202-207209.
65. A.B. Shick, O.N. Mryasov. Coulomb correlations and magnetic anisotropy in ordered L 1 0 CoPt and FePt alloys. Physical Review B. 2003, 67(17), 172407-172412.
66. G. Armelles, D. Weller, B. Rellinghaus, R. Farrow, M. Toney, P. Caro, et al. Origin of strong intrinsic Kerr effect in FePt and FePd ordered compounds. IEEE Transactions on Magnetics. 1997, 33(5), 3220-3222.
67. C. Fang, M. Zhang. Multifunctional magnetic nanoparticles for medical imaging applications. Journal of Materials Chemistry. 2009, 19(35), 6258-6266.
68. M. Mahmoudi, S. Sant, B. Wang, S. Laurent, T. Sen. Superparamagnetic iron oxide nanoparticles (SPIONs): development, surface modification and applications in chemotherapy. Advanced Drug Delivery Reviews. 2011, 63(1), 24-46.

69. L. Li, W. Jiang, K. Luo, H. Song, F. Lan, Y. Wu, et al. Superparamagnetic iron oxide nanoparticles as MRI contrast agents for non-invasive stem cell labeling and tracking. Theranostics. 2013, 3(8), 595-599.
70. E. Amstad, M. Textor, E. Reimhult. Stabilization and functionalization of iron oxide nanoparticles for biomedical applications. Nanoscale. 2011, 3(7), 2819-2843.
71. C. Xu, S. Sun. Superparamagnetic nanoparticles as targeted probes for diagnostic and therapeutic applications. Dalton Transactions. 2009, (29), 5583-5591.
72. L. Hajbaa, A. Guttman, The use of magnetic nanoparticles in cancer theranostics: Toward handheld diagnostic devices. Biotechnology Advances. 2016, 34, 354–361.
73. S.-W. Chou, Y.-H. Shau, P.-C. Wu, Y.-S. Yang, D.-B. Shieh, C.-C. Chen. *In vitro* and *in vivo* studies of FePt nanoparticles for dual modal CT/MRI molecular imaging. Journal of the American Chemical Society. 2010, 132(38), 13270-13278.
74. S. Chen, L. Wang, S.L. Duce, S. Brown, S. Lee, A. Melzer, et al. Engineered biocompatible nanoparticles for in vivo imaging applications. Journal of the American Chemical Society. 2010, 132(42), 15022-15029.
75. Shi, Y., Lin, M., Jiang, X., & Liang, S. Recent advances in FePt nanoparticles for biomedicine. Journal of Nanomaterials. 2015, 2015 (2015). http://dx.doi.org/10.1155/2015/467873
76. M. Monteforte, S. Kobayashi, L. D .Tung, K. Higashimine, D. M. Mott, S. Maenosono, N. T. K. Thanh, I. K. Robinson, Quantitative two-dimensional strain mapping of small core–shell FePt@Fe_3O_4 nanoparticles, New Journal of Physic. 2016, 18, 033016-033021
77. T. Fuchigami, R. Kawamura, Y. Kitamoto, M. Nakagawa, Y. Namiki. Ferromagnetic FePt-nanoparticles/polycation hybrid capsules designed for a magnetically guided drug delivery system. Langmuir. 2011, 27(6), 2923-2928.
78. N. Lewinski, V. Colvin, R. Drezek. Cytotoxicity of nanoparticles. Small. 2008, 4(1), 26-49.
79. S. Chen, L. Wang, S.L. Duce, S. Brown, S. Lee, A. Melzer, et al. Engineered biocompatible nanoparticles for in vivo imaging applications. Journal of the American Chemical Society. 2010, 132(42), 15022-15029.

80. S.-W. Chou, Y.-H. Shau, P.-C. Wu, Y.-S. Yang, D.-B. Shieh, C.-C. Chen. In vitro and in vivo studies of FePt nanoparticles for dual modal CT/MRI molecular imaging. Journal of the American Chemical Society. 2010, 132(38), 13270-13278.
81. K.M. Krishnan. Biomedical nanomagnetics: a spin through possibilities in imaging, diagnostics, and therapy. IEEE transactions on magnetics. 2010, 46(7), 2523-2558.
82. S. Liang, Q. Zhou, M. Wang, Y. Zhu, Q. Wu, X. Yang. Water-soluble l-cysteine-coated FePt nanoparticles as dual MRI/CT imaging contrast agent for glioma. International Journal of Nanomedicine. 2015,10, 2325-2333.
83. P.C. Naha, A. Al Zaki, E. Hecht, M. Chorny, P. Chhour, E. Blankemeyer, et al. Dextran coated bismuth–iron oxide nanohybrid contrast agents for computed tomography and magnetic resonance imaging. Journal of Materials Chemistry B. 2014, 2(46), 8239-8248.
84. P.C. Naha, A. Al Zaki, E. Hecht, M. Chorny, P. Chhour, E. Blankemeyer, et al. Dextran coated bismuth–iron oxide nanohybrid contrast agents for computed tomography and magnetic resonance imaging. Journal of Materials Chemistry B. 2014, 2(46), 8239-8248.
85. N.K. Devaraj, E.J. Keliher, G.M. Thurber, M. Nahrendorf, R. Weissleder. 18F labeled nanoparticles for in vivo PET-CT imaging. Bioconjugate Chemistry. 2009, 20(2), 397-401.
86. R.A. Revia, M. Zhang. Magnetite nanoparticles for cancer diagnosis, treatment, and treatment monitoring: recent advances. Materials Today. 2016, 19(3), 157-168.
87. D. Li, X. Tang, B. Pulli, C. Lin, P. Zhao, J. Cheng, et al. Theranostic nanoparticles based on bioreducible polyethylenimine-coated iron oxide for reduction-responsive gene delivery and magnetic resonance imaging. International Journal of Nanomedicine. 2014, 9, 3347-3361.
88. F.M. Kievit, Z.R. Stephen, K. Wang, C.J. Dayringer, J.G. Sham, R.G. Ellenbogen, et al. Nanoparticle mediated silencing of DNA repair sensitizes pediatric brain tumor cells to γ-irradiation. Molecular Oncology. 2015, 9(6), 1071-1080.
89. J. Kolosnjaj-Tabi, R. Di Corato, L. Lartigue, I. Marangon, P. Guardia, A.K. Silva, et al. Heat-generating iron oxide nanocubes: subtle “destructurators” of the tumoral microenvironment. ACS Nano. 2014, 8(5), 4268-4283.
90. S.H. Hu, B.J. Liao, C.S. Chiang, P.J. Chen, I.W. Chen, S.Y. Chen. Core-Shell Nanocapsules Stabilized by Single-Component Polymer and Nanoparticles for Magneto-

Chemotherapy/Hyperthermia with Multiple Drugs. Advanced Materials. 2012, 24(27),3627-3632.

91. D.K. Kirui, D.A. Rey, C.A. Batt. Gold hybrid nanoparticles for targeted phototherapy and cancer imaging. Nanotechnology. 2010, 21(10), 105105-105110.
92. M. Nafiujjaman, V. Revuri, M. Nurunnabi, K.J. Cho, Y.-k. Lee. Photosensitizer conjugated iron oxide nanoparticles for simultaneous in vitro magneto-fluorescent imaging guided photodynamic therapy. Chemical Communications. 2015, 51(26), 5687-5690.
93. Z. Li, C. Wang, L. Cheng, H. Gong, S. Yin, Q. Gong, et al. PEG-functionalized iron oxide nanoclusters loaded with chlorin e6 for targeted, NIR light induced, photodynamic therapy. Biomaterials. 2013, 34(36), 9160-9170.
94. J. Huang, X. Zhong, L. Wang, L. Yang, H. Mao. Improving the magnetic resonance imaging contrast and detection methods with engineered magnetic nanoparticles. Theranostics. 2012, 2(1), 86-102.
95. J. Gao, H. Gu, B. Xu. Multifunctional magnetic nanoparticles: design, synthesis, and biomedical applications. Accounts of Chemical Research. 2009, 42(8), 1097-1107.
96. S.-M. Lai, T.-Y. Tsai, C.-Y. Hsu, J.-L. Tsai, M.-Y. Liao, P.-S. Lai. Bifunctional silica-coated superparamagnetic FePt nanoparticles for fluorescence/MR dual imaging. Journal of Nanomaterials. 2012, 2012, 5-13.
97. J. Gao, B. Zhang, Y. Gao, Y. Pan, X. Zhang, B. Xu. Fluorescent magnetic nanocrystals by sequential addition of reagents in a one-pot reaction: a simple preparation for multifunctional nanostructures. Journal of the American Chemical Society. 2007, 129(39), 11928-11935.
98. R.M. Taylor, D.L. Huber, T.C. Monson, A.-M.S. Ali, M. Bisoffi, L.O. Sillerud. Multifunctional iron platinum stealth immunomicelles: targeted detection of human prostate cancer cells using both fluorescence and magnetic resonance imaging. Journal of Nanoparticle Research. 2011, 13(10), 4717-4729.
99. S. Maenosono, S. Saita. Theoretical assessment of FePt nanoparticles as heating elements for magnetic hyperthermia. IEEE Transactions on Magnetics. 2006, 42(6), 1638-1642.

100. K.M. Seemann, M. Luysberg, Z. Révay, P. Kudejova, B. Sanz, N. Cassinelli, et al. Magnetic heating properties and neutron activation of tungsten-oxide coated biocompatible FePt core–shell nanoparticles. Journal of Controlled Release. 2015,197, 131-137.

101. C.-L. Chen, L.-R. Kuo, S.-Y. Lee, Y.-K. Hwu, S.-W. Chou, C.-C. Chen, et al. Photothermal cancer therapy via femtosecond-laser-excited FePt nanoparticles. Biomaterials. 2013, 34(4), 1128-1134.

102. T. Fuchigami, R. Kawamura, Y. Kitamoto, M. Nakagawa, Y. Namiki. A magnetically guided anti-cancer drug delivery system using porous FePt capsules. Biomaterials. 2012, 33(5), 1682-1687.

103. Y. Liu, K. Yang, L. Cheng, J. Zhu, X. Ma, H. Xu, et al. PEGylated FePt@ Fe_2O_3 core-shell magnetic nanoparticles: potential theranostic applications and in vivo toxicity studies. Nanomedicine: Nanotechnology, Biology and Medicine. 2013, 9(7), 1077-1088.

104. J. Gao, G. Liang, B. Zhang, Y. Kuang, X. Zhang, B. Xu. FePt@ CoS2 yolk− shell nanocrystals as a potent agent to kill HeLa cells. Journal of the American Chemical Society. 2007, 129(5), 1428-1433.

105. C. Xu, Z. Yuan, N. Kohler, J. Kim, M.A. Chung, S. Sun. FePt nanoparticles as an Fe reservoir for controlled Fe release and tumor inhibition. Journal of the American Chemical Society. 2009, 131(42), 15346-15351.

106. R. Kawashima, M. Uchida, T. Yamaki, K. Ohtake, T. Hatanaka, H. Uchida, et al. Development of a Transnasal Delivery System for Recombinant Human Growth Hormone (rhGH): Effects of the Concentration and Molecular Weight of Poly-L-arginine on the Nasal Absorption of rhGH in Rats. Biological and Pharmaceutical Bulletin. 2016, 39(3), 329-335.

107. T. Yang, A. Hussain, S. Bai, I.A. Khalil, H. Harashima, F. Ahsan. Positively charged polyethylenimines enhance nasal absorption of the negatively charged drug, low molecular weight heparin. Journal of Controlled Release. 2006, 115(3), 289-297.

108. N. Oku, N. Yamaguchi, N. Yamaguchi, S. Shibamoto, F. Ito, M. Nango. The fusogenic effect of synthetic polycations on negatively charged lipid bilayers. The Journal of Biochemistry. 1986, 100(4), 935-944.

109. M.P. Xiong, M.L. Forrest, G. Ton, A. Zhao, N.M. Davies, G.S. Kwon. Poly (aspartate-g-PEI800), a polyethylenimine analogue of low toxicity and high transfection efficiency for gene delivery. Biomaterials. 2007, 28(32), 4889-4900.

110. D. Fischer, T. Bieber, Y. Li, H.-P. Elsässer, T. Kissel. A novel non-viral vector for DNA delivery based on low molecular weight, branched polyethylenimine: effect of molecular weight on transfection efficiency and cytotoxicity. Pharmaceutical Research. 1999, 16(8), 1273-1279.

111. A. Beyerle, M. Irmler, J. Beckers, T. Kissel, T. Stoeger. Toxicity pathway focused gene expression profiling of PEI-based polymers for pulmonary applications. Molecular Pharmaceutics. 2010, 7(3), 727-737.

112. G. Grandinetti, N.P. Ingle, T.M. Reineke. Interaction of poly (ethylenimine)–DNA polyplexes with mitochondria: implications for a mechanism of cytotoxicity. Molecular Pharmaceutics. 2011, 8(5), 1709-1719.

113. S. Prijic, G. Sersa. Magnetic nanoparticles as targeted delivery systems in oncology. Radiology and Oncology. 2011, 45(1), 1-16.

114. D. Li, X. Tang, B. Pulli, C. Lin, P. Zhao, J. Cheng, et al. Theranostic nanoparticles based on bioreducible polyethylenimine-coated iron oxide for reduction-responsive gene delivery and magnetic resonance imaging. International Journal of Nanomedicine. 2014, 9, 3347-3361.

115. H. Yoo, S.-K. Moon, T. Hwang, Y.S. Kim, J.-H. Kim, S.-W. Choi, et al. Multifunctional magnetic nanoparticles modified with polyethylenimine and folic acid for biomedical theranostics. Langmuir. 2013, 29(20), 5962-5967

116. I. I. Slowing, J. L. Vivero-Escoto, C.-W. Wu, V. S.-Y. Lin. Mesoporous silica nanoparticles as controlled release drug delivery and gene transfection carriers. Advanced Drug Delivery Reviews. 2008, 60(11), 1278-1288.

117. E. Chaum, M.P. Hatton, G. Stein. Polyplex-mediated gene transfer into human retinal pigment epithelial cells in vitro. Journal of Cellular Biochemistry. 2000, 76(1), 153-160.

118. R. Khar, G. Jain, M. Warsi, N. Mallick, S. Akhter, S. Pathan, et al. Nano-vectors for the ocular delivery of nucleic acid-based therapeutics. Indian Journal of Pharmaceutical Sciences. 2010, 72(6), 675-681.

119. A.M. Maguire, F. Simonelli, E.A. Pierce, E.N. Pugh Jr, F. Mingozzi, J. Bennicelli, et al. Safety and efficacy of gene transfer for Leber's congenital amaurosis. New England Journal of Medicine. 2008, 358(21), 2240-2248.

120. J.-H. Kang, Y. Tachibana, W. Kamata, A. Mahara, M. Harada-Shiba, T. Yamaoka. Liver-targeted siRNA delivery by polyethylenimine (PEI)-pullulan carrier. Bioorganic & Medicinal Chemistry. 2010, 18(11), 3946-3950.

121. S. Askarian, K. Abnous, M. Darroudi, R.K. Oskuee, M. Ramezani. Gene delivery to neuroblastoma cells by poly (L-lysine)-grafted low molecular weight polyethylenimine copolymers. Biologicals. 2016, 44(4), 212-218.

122. A. Ewe, S. Przybylski, J. Burkhardt, A. Janke, D. Appelhans, A. Aigner. A novel tyrosine-modified low molecular weight polyethylenimine (P10Y) for efficient siRNA delivery in vitro and in vivo. Journal of Controlled Release. 2016, 230, 13-25.

123. S.J. Fox, Fazil, C. Dhand, M. Venkatesh, E.T.L. Goh, S. Harini, et al. Insight into membrane selectivity of linear and branched polyethylenimines and their potential as biocides for advanced wound dressings. Acta Biomaterialia. 2016, 37, 155-64.

124. Y. Xie, N.H. Kim, V. Nadithe, D. Schalk, A. Thakur, A. Kılıç, et al. Targeted delivery of siRNA to activated T cells via transferrin-polyethylenimine (Tf-PEI) as a potential therapy of asthma. Journal of Controlled Release. 2016, 229, 120-129.

125. S. Taghavi, A. HashemNia, F. Mosaffa, S. Askarian, K. Abnous, M. Ramezani. Preparation and evaluation of polyethylenimine-functionalized carbon nanotubes tagged with 5TR1 aptamer for targeted delivery of Bcl-xL shRNA into breast cancer cells. Colloids and Surfaces B: Biointerfaces. 2016, 140, 28-39.

126. Y. Tan, L. Xie, Z. Wang, N. Zhang, C. Zou, Z.-y. Chen, et al. Epsilon-caprolactone modified polyethylenimine for highly efficient antigen delivery and chemical exchange saturation transfer functional MR imaging. Biomaterials. 2015, 56, 219-228.

127. C. Dempsey, I. Lee, K.R. Cowan, J. Suh. Coating barium titanate nanoparticles with polyethylenimine improves cellular uptake and allows for coupled imaging and gene delivery. Colloids and Surfaces B: Biointerfaces. 2013, 112, 108-12.

128. S.-J. Kim, H. Ise, E. Kim, M. Goto, T. Akaike, B.H. Chung. Imaging and therapy of liver fibrosis using bioreducible polyethylenimine/siRNA complexes conjugated with N-acetylglucosamine as a targeting moiety. Biomaterials. 2013, 34(27),6504-14.

129. C. Ma, X. Zhang, L. Yang, Y. Wu, H. Liu, X. Zhang, et al. Preparation of fluorescent organic nanoparticles from polyethylenimine and sucrose for cell imaging. Materials Science and Engineering: C. 2016, 68,37-42.

130. Y. Ding, S.Z. Shen, H. Sun, K. Sun, F. Liu, Y. Qi, et al. Design and construction of polymerized-chitosan coated Fe_3O_4 magnetic nanoparticles and its application for hydrophobic drug delivery. Materials Science and Engineering: C. 2015, 48,487-98.

131. J. Huang, Q. Shu, L. Wang, H. Wu, A.Y. Wang, H. Mao. Layer-by-layer assembled milk protein coated magnetic nanoparticle enabled oral drug delivery with high stability in stomach and enzyme-responsive release in small intestine. Biomaterials. 2015, 39,105-113.

132. S. Kossatz, J. Grandke, P. Couleaud, A. Latorre, A. Aires, K. Crosbie-Staunton, et al. Efficient treatment of breast cancer xenografts with multi-functionalized iron oxide nanoparticles combining magnetic hyperthermia and anti-cancer drug delivery. Breast Cancer Research. 2015, 17(1), 66-74.

133. P.J. Kempen, S. Greasley, K.A. Parker, J.L. Campbell, H.-Y. Chang, J.R. Jones, et al. Theranostic mesoporous silica nanoparticles biodegrade after pro-survival drug delivery and ultrasound/magnetic resonance imaging of stem cells. Theranostics. 2015, 5(6), 631-639.

134. E. Ebrahimi, A. Akbarzadeh, E. Abbasi, A.A. Khandaghi, F. Abasalizadeh, S. Davaran. Novel drug delivery system based on doxorubicin-encapsulated magnetic nanoparticles modified with PLGA-PEG1000 copolymer. Artificial Cells, Nanomedicine, and Biotechnology. 2016, 44(1), 290-297.

135. S. N. abatabaei, H. Girouard H, A. S. Carret, S. Martel, Remote control of the permeability of the blood-brain barrier by magnetic heating of nanoparticles: A proof of concept for brain drug delivery, Journal of Controlled Release. 2015, 206, 49-57.

136. S. Patra, E. Roy, P. Karfa, S. Kumar, R. Madhuri, P.K. Sharma. Dual-responsive polymer coated superparamagnetic nanoparticle for targeted drug delivery and hyperthermia treatment. ACS Applied Materials & Interfaces. 2015, 7(17), 9235-9246.

137. A.R. Chowdhuri, D. Bhattacharya, S.K. Sahu. Magnetic nanoscale metal organic frameworks for potential targeted anticancer drug delivery, imaging and as an MRI contrast agent. Dalton Transactions. 2016, 45(7), 2963-2973.

138. N.S. Elbialy, M.M. Fathy, W.M. Khalil. Doxorubicin loaded magnetic gold nanoparticles for in vivo targeted drug delivery. International Journal of Pharmaceutics. 2015, 490(1), 190-199.

139. X.-L. Qiu, Q.-L. Li, Y. Zhou, X.-Y. Jin, A.-D. Qi, Y.-W. Yang. Sugar and pH dual-responsive snap-top nanocarriers based on mesoporous silica-coated Fe 3 O 4 magnetic nanoparticles for cargo delivery. Chemical Communications. 2015, 51(20), 4237-4240.

140. H. Hashemi-Moghaddam, S. Kazemi-Bagsangani, M. Jamili, S. Zavareh. Evaluation of magnetic nanoparticles coated by 5-fluorouracil imprinted polymer for controlled drug delivery in mouse breast cancer model. International Journal of Pharmaceutics. 2016, 497(1), 228-238.

141. J. Zhao, C. Lu, X. He, X. Zhang, W. Zhang, X. Zhang. Polyethylenimine-grafted cellulose nanofibril aerogels as versatile vehicles for drug delivery. ACS Applied Materials & Interfaces. 2015, 7(4), 2607-2615.

142. G. Zhang, J. Gao, J. Qian, L. Zhang, K. Zheng, K. Zhong, et al. Hydroxylated Mesoporous Nanosilica Coated by Polyethylenimine Coupled with Gadolinium and Folic Acid: A Tumor-Targeted T 1 Magnetic Resonance Contrast Agent and Drug Delivery System. ACS Applied Materials & Interfaces. 2015, 7(26), 14192-14200.

143. M. Mohammadi, Z. Salmasi, M. Hashemi, F. Mosaffa, K. Abnous, M. Ramezani. Single-walled carbon nanotubes functionalized with aptamer and piperazine–polyethylenimine derivative for targeted siRNA delivery into breast cancer cells. International Journal of Pharmaceutics. 2015, 485(1), 50-60.

144. L. Liu, M. Zheng, D. Librizzi, T. Renette, O.M. Merkel, T. Kissel. Efficient and Tumor Targeted siRNA Delivery by Polyethylenimine-graft-polycaprolactone-block-poly (ethylene glycol)-folate (PEI–PCL–PEG–Fol). Molecular Pharmaceutics. 2015, 13(1), 134-143.

145. S. Taghavi, A.H. Nia, K. Abnous, M. Ramezani. Polyethylenimine-functionalized carbon nanotubes tagged with AS1411 aptamer for combination gene and drug delivery

into human gastric cancer cells. International Journal of Pharmaceutics. 2017, 516(1), 301-312.

146. M. Wang, T. Liu, L. Han, W. Gao, S. Yang, N. Zhang. Functionalized O-carboxymethyl-chitosan/polyethylenimine based novel dual pH-responsive nanocarriers for controlled co-delivery of DOX and genes. Polymer Chemistry. 2015, 6(17), 3324-3335.

147. Y.-L. Lo, H.-L. Chou, Z.-X. Liao, S.-J. Huang, J.-H. Ke, Y.-S. Liu, et al. Chondroitin sulfate-polyethylenimine copolymer-coated superparamagnetic iron oxide nanoparticles as an efficient magneto-gene carrier for microRNA-encoding plasmid DNA delivery. Nanoscale. 2015, 7(18), 8554-8565.

148. L.N. Borgheti-Cardoso, L.V. Depieri, S.A. Kooijmans, H. Diniz, R.A.J. Calzzani, F.T.M. de Carvalho Vicentini, et al. An in situ gelling liquid crystalline system based on monoglycerides and polyethylenimine for local delivery of siRNAs. European Journal of Pharmaceutical Sciences. 2015, 74,103-117.

149. J.-M. Li, W. Zhang, H. Su, Y.-Y. Wang, C.-P. Tan, L.-N. Ji, et al. Reversal of multidrug resistance in MCF-7/Adr cells by codelivery of doxorubicin and BCL2 siRNA using a folic acid-conjugated polyethylenimine hydroxypropyl-β-cyclodextrin nanocarrier. International Journal of Nanomedicine. 2015,10,3147-3152.

150. G. Yang, H. Gong, T. Liu, X. Sun, L. Cheng, Z. Liu. Two-dimensional magnetic WS 2@ Fe 3 O 4 nanocomposite with mesoporous silica coating for drug delivery and imaging-guided therapy of cancer. Biomaterials. 2015,60, 62-71.

151. M. Das, W. Duan, S.K. Sahoo. Multifunctional nanoparticle–EpCAM aptamer bioconjugates: A paradigm for targeted drug delivery and imaging in cancer therapy. Nanomedicine: Nanotechnology, Biology and Medicine. 2015, 11(2), 379-389.

152. G. Tian, X. Zheng, X. Zhang, W. Yin, J. Yu, D. Wang, et al. TPGS-stabilized NaYbF 4: Er upconversion nanoparticles for dual-modal fluorescent/CT imaging and anticancer drug delivery to overcome multi-drug resistance. Biomaterials. 2015, 40,107-116.

153. T. Kang, F. Li, S. Baik, W. Shao, D. Ling, T. Hyeon. Surface design of magnetic nanoparticles for stimuli-responsive cancer imaging and therapy. Biomaterials. 2017, 136, 98-114.

154. M. Patitsa, K. Karathanou, Z. Kanaki, L. Tzioga, N. Pippa, C. Demetzos, et al. Magnetic nanoparticles coated with polyarabic acid demonstrate enhanced drug delivery and imaging properties for cancer theranostic applications. Scientific Reports. 2017,7, 775-783

155. H. Chen, X. Sun, G.D. Wang, K. Nagata, Z. Hao, A. Wang, et al. LiGa 5 O 8: Cr-based theranostic nanoparticles for imaging-guided X-ray induced photodynamic therapy of deep-seated tumors. Materials Horizons. 2017. Doi:10.1039/C7MH00442G

156. D. Alberti, N. Protti, M. Franck, R. Stefania, S. Bortolussi, S. Altieri, et al. Theranostic nanoparticles loaded with imaging probes and rubrocurcumin for combined cancer therapy by folate receptor targeting. ChemMedChem. 2017, 12(7), 502-509.

157. A. Nagesetti, S. Srinivasan, A.J. McGoron. Polyethylene glycol modified ORMOSIL theranostic nanoparticles for triggered doxorubicin release and deep drug delivery into ovarian cancer spheroids. Journal of Photochemistry and Photobiology B: Biology. 2017, 174, 209-216.

158. F. Mohammad, H.A. Al-Lohedan. Luteinizing hormone-releasing hormone targeted superparamagnetic gold nanoshells for a combination therapy of hyperthermia and controlled drug delivery. Materials Science and Engineering: C. 2017, 76,692-700.

159. N. Gao, E.N. Bozeman, W. Qian, L. Wang, H. Chen, M. Lipowska, et al. Tumor Penetrating Theranostic Nanoparticles for Enhancement of Targeted and Image-guided Drug Delivery into Peritoneal Tumors following Intraperitoneal Delivery. Theranostics. 2017, 7(6), 1689-1704.

160. N. Gao, E.N. Bozeman, W. Qian, L. Wang, H. Chen, M. Lipowska, et al. Tumor Penetrating Theranostic Nanoparticles for Enhancement of Targeted and Image-guided Drug Delivery into Peritoneal Tumors following Intraperitoneal Delivery. Theranostics. 2017, 7(6), 1689-1694.

161. Y.-H. Chi, J.-K. Hsiao, M.-H. Lin, C. Chang, C.-H. Lan, H.-C. Wu. Lung Cancer-Targeting Peptides with Multi-subtype Indication for Combinational Drug Delivery and Molecular Imaging. Theranostics. 2017, 7(6), 1612-1632.

162. Z. Lu, F.-Y. Huang, R. Cao, Y.-Y. Lin, S. Zhou, H. Zhao, et al. Synthesis of mPEG-dBSA-Cy5. 5 Nanoparticles for Tumor Imaging and Drug Delivery. Nanoscience and Nanotechnology Letters. 2017, 9(2), 184-189.

163. L. Chen, X. Zhou, W. Nie, W. Feng, Q. Zhang, W. Wang, et al. Marriage of Albumin− gadolinium complexes and mos2 nanoflakes as cancer theranostics for dual-modality magnetic resonance/photoacoustic imaging and photothermal therapy. ACS Applied Materials & Interfaces. 2017, 9 (21),17786–17798

164. S. Zhang, W. Guo, J. Wei, C. Li, X.-J. Liang, M. Yin. Terrylenediimide-based intrinsic theranostic nanomedicines with high photothermal conversion efficiency for photoacoustic imaging-guided cancer therapy. ACS nano. 2017, 11(4), 3797-3805.

165. J. Chen, S. Ratnayaka, A. Alford, V. Kozlovskaya, F. Liu, B. Xue, et al. Theranostic multilayer capsules for ultrasound imaging and guided drug delivery. ACS nano. 2017, 11(3), 3135-3146.